Supplement to Chapter 9

This document contains material that is ancillary to Chapter 9 of the CCMVal ozone report. The material is divided into three sections. The first section provides a more complete set of TSAM diagnostics for the five latitude bands discussed in Chapter 9. The second section investigates the sensitivity of the TSAM analysis, and its prediction of return dates, to the elimination of an outlying model. The final section investigates the application of 1:2:1 smoothing to individual model ensemble time series in the definition of a multi-model ensemble mean and performs a direct comparison with the results of the TSAM analysis.

9S.1 TSAM Latitude-Band Diagnostics

In this section we present a more complete set of figures associated with the application of the TSAM analysis to the time series of total column ozone and 50hPa inorganic Cly in the 5 latitude bands discussed in Chapter 9. For each of these two types of time series, and in each latitude band, a set of 4 figures is presented.

The first and second figures in the set provide a comparison of CCMVal-1 vs CCMVal-2 (e.g. Fig. 9S.1 and 9S.2). The first shows four panels in which the two panels on the left display raw time series data with their initial individual model trend (IMT) estimates and the two panels on the right display 1980 baseline-adjusted time series data with their 1980 baseline-adjusted IMT estimates. The second figure provides a comparison of 1980 baseline adjusted IMT and multi-model trend (MMT) estimates with 95% confidence and 95% prediction intervals.

The third and fourth figures in the set focus on CCMVal-2 and investigate the use of the earlier reference dates of 1970 and 1960 for the baseline adjustment in the TSAM analysis. The third figure shows the 1970 and 1960 baseline-adjusted time series data and baseline-adjusted IMT estimates for the TSAM analysis (e.g. Fig. 9S.3). The fourth figure displays the 1970 and 1960 baseline-adjusted IMT and MMT estimates along with 95% confidence and 95% prediction intervals (e.g. Fig. 9S.4).

In the first figure of this set, the range along the vertical axis has been forced to be identical in each of the four panels (e.g. Fig. 9S.1). In this way the collapse of the data arising from the application of the baseline adjustment (left to right) and differences between CCMVal-1 and CCMVal-2 (top to bottom) can be visually identified. In nearly all latitude bands, it is seen that there exists a large inter-model spread in the raw time series that is not apparent in the baseline adjusted time series, which form the primary diagnostic considered in Chapter 9. In at least one instance, the baseline adjusted time series would seem to show CCMVal-2 to have less model-spread than CCMVal-1 while the raw time series indicates the opposite behaviour (i.e. Fig. 9S.17). For this reason it is important to have plots of this nature for all of the latitude bands discussed in Chapter 9.

9S.2 Sensitivity to Outliers

As described in the Appendix to Chapter 9, the TSAM analysis allows the specification of prior weights for individual models based on quantitative performance metrics. The expectation was that such performance based weighting might reduce the sensitivity of the final multi-model average to the presence of outliers. For this report, however, it was decide that quantitative performance metrics were not as yet sufficiently robust to be useful for prior weighting of the models. Even so, it is of interest to investigate the sensitivity of the TSAM analysis to outlying models. In this section, we employ an extreme limit of performance-based weighting by arbitrarily removing one model from the TSAM analysis. For this sensitivity experiment, we have selected the UMUKCA-METO model which displayed anomalously large 50hPa Cly in all latitude bands.

The impact of removing the UMUKCA-METO model on the evolution of total column O_3 is considered first. While the UMUKCA-METO model is an outlier with respect to 50hPa Cly, its column O_3 is within the main spread of models. Consequently, for column O_3, the removal of UMUKCA-METO tests the sensitivity of the TSAM analysis to the removal of a model that is not an outlier. In Fig. 9S.41 MMT estimates for total Column O_3 in the 5 latitude bands considered in Chapter 9 are presented for the two cases of the TSAM analyses applied to all models (right column) and the TSAM applied to all models except UMUKCA.METO (left column). Inspection of Fig. 9S.41 shows the MMT estimates and 95% confidence and prediction intervals for all latitude bands to be very similar in both cases. This is verified in Fig. 9S.42 where the MMT estimate with UMUKCA-METO removed (blue) is overlayed on the MMT estimate derived from all models (dark grey). For total column O_3 the two cases are essentially indistinguishable. A test of the impact on 1980 return dates, Fig. 9S.43, shows no difference between the two cases. From this we may conclude that, for the CCMVal-2 model set, the TSAM analysis is insensitive to the removal of a model that is not an outlier.

The sensitivity of the TSAM analysis of 50hPa Cly to the removal of UMUKCA-METO is a more severe test as the 50hPa Cly of UMUKCA-METO is a significant outlier in all latitude bands. In Fig. 9S.44 MMT estimates for 50hPa Cly in the 5 latitude bands are presented for the two cases of the TSAM analyses applied to all models (right column) and to all models except UMUKCA.METO (left column). Again, the MMT estimates and the 95% confidence and prediction intervals, for all latitude bands, appears very similar in both cases. It is only when the MMT estimates in both cases are overlain, Fig. 9S.45, that differences become apparent. The largest difference is found in the Arctic (60°N-90°N) where the removal of UMUKCA-METO causes a reduction in the MMT estimate of 50hPa Cly. While this seems significant, the impact on return dates remains within the confidence intervals of the original TSAM analysis (Fig. 9S.46). This suggests that, for the CCMVal-2 model set, predictions based on the TSAM analysis are robust to the removal of one of the largest model outliers.

The sensitivity experiments in this section suggest that, for the CCMVal-2 model set, the application of prior weights based on quantitative performance metrics would not significantly alter predictions based on the TSAM analysis.

9S.3 1:2:1 Smoothing vs the TSAM Analysis

Previous studies of CCMVal-1 time series determined smooth trends in the data by employing a simple 1:2:1 filter [WMO 2007, Eyring et al. 2007]. As described in Chapter 9, the TSAM analysis is based on a statistical framework employing a nonparametric additive model to determine smooth IMT and MMT estimates from the time series. In addition to the ability to make formal inference (e.g. calculation of confidence and prediction intervals), it was suggested that the TSAM analysis was also advantageous because it allowed the formulation of MMT estimates for the full REF2 period from model time series data that sampled only portions of this period. While this is critical for the analysis of the CCMVal-1 time series data, it is less critical for the CCMVal-2 time series data as nearly all models in CCMVal-2 provided time series than spanned the full range of 1960-2099. Given a sufficient number of models, the expectation is that a straight multi-model average of the time series should produce a MMT estimate that is very close to the TSAM MMT estimate. Here we investigate this question for the CCMVal-2 model set employing 1:2:1 filtering of individual model time series in the derivation of the multi-model average.

There were two issues which complicated the application of a straight multi-model average of the CCMVal-2 REF-B2 time series. Two of the thirteen models did not provide time series for the full REF-B2 period of 1960-2099. GEOSCCM provided only 2000-2099 and UMUKCA-METO provided 1960-2084. For the case of the GEOSCCM, in Chapter 9, the data from the REF-B1 experiment spanning 1960-2004 was included in the TSAM analysis to have GEOSCCM data cover the complete REF-B2 period. The GEOSCCM REF-B1 and REF-B2 time series are not really ensemble members as they overlap only over the range 2000-2004. Here it was decided to average the two over the this range to produce one time series which spanned 1960-2099. While this produced small kinks in the GEOSCCM time series at 2000 and 2004, it was found not to cause kinks in the multi-model average time series.

For the case of UMUKCA-METO, its sudden termination at 2084 causes a kink in a straight multi-model average as the equal weights of 1/13 for each model switch suddenly to 1/12 at this point. In the end it was decided to use the prior weighting that produced quadratic tapering towards the ends of the time series that was introduced in Section 9A.4 of the appendix to Chapter 9 (equations 9.20 and 9.21). A multi-model average of time series which span the entire period would not be affected by the introduction of the quadratic tapering. Only models that do not span the entire period would see their contribution to the multi-model mean diminish towards the ends of their time series. As in the TSAM analysis, this proved to be very effective at eliminating discontinuities in the multi-model trend estimate.

In Fig. 9S.47 the IMT estimates of column ozone in 5 latitude bands derived from a 1:2:1 filter applied 30 times to each model time series (left) is compared to the IMT estimates derived from the TSAM analysis (right). The MMT estimates for each approach is displayed in this figure and Fig. 9S.48. While the IMT estimates derived from the TSAM approach are much smoother than those derived using 1:2:1 filtering, the MMT estimates appear nearly identical for each approach. This is further verified in Fig. 9S.49 where a comparison of total column ozone 1980 return dates for each method is presented. The MMT return dates derived from 1:2:1 filtered model time series are essentially identical to those derived from the TSAM approach. The IMT return dates generally display a larger spread for the 1:2:1 filtering since these are less smooth than the IMT estimates produced by the TSAM approach (Fig. 9S.47). Similar conclusions apply to the analysis of 50hPa Cly which is presented in Figs. 9S.50-9S.52.

The conclusion here is that, for the CCMVal-2 data set, multi-model averaged time series produced from 1:2:1 filtered individual model time series are consistent with the MMT estimate of the more sophisticated TSAM analysis. However, the use of 1:2:1 filtering does not provide confidence and prediction intervals for the multi-model average as it is not based on a statistical model. The use of 1:2:1 filtering to investigate IMT estimates is less robust as the 1:2:1 filter leaves significant structure in the individual model time series compared to the IMT estimates of the TSAM approach.

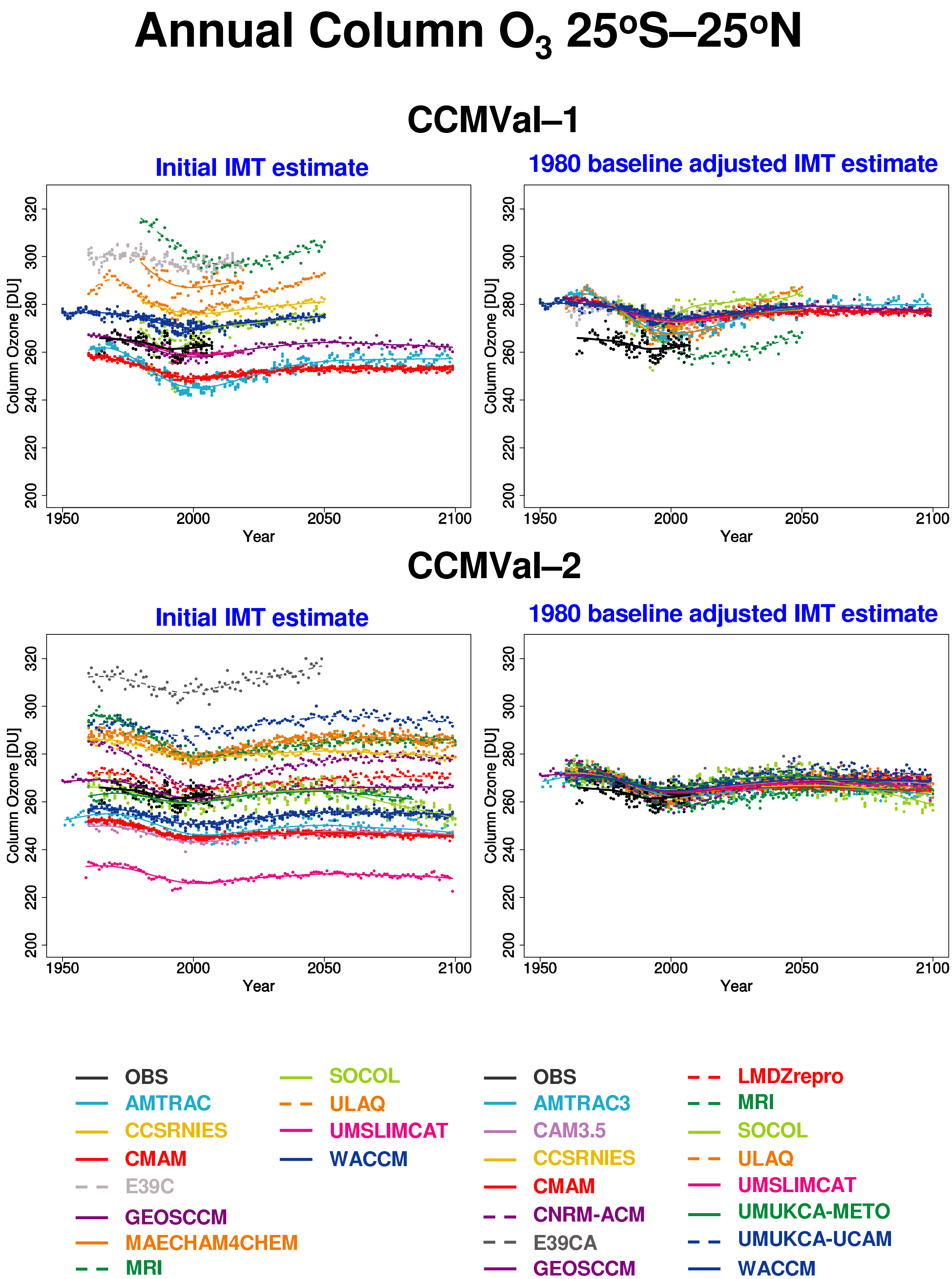

Figure 9S.1: Raw time series data of annually averaged Column O_3 (25°S-25°N) and initial individual model trend (IMT) estimates (left-hand panels), and 1980 baseline-adjusted time series data and IMT estimates (right-hand panels) for the TSAM analysis of CCMVal-1 (top) and CCMVal-2 (bottom). Observation data (black) and lowess fit (with smoother span f=0.4) to the observations appears as a black line in all panels.

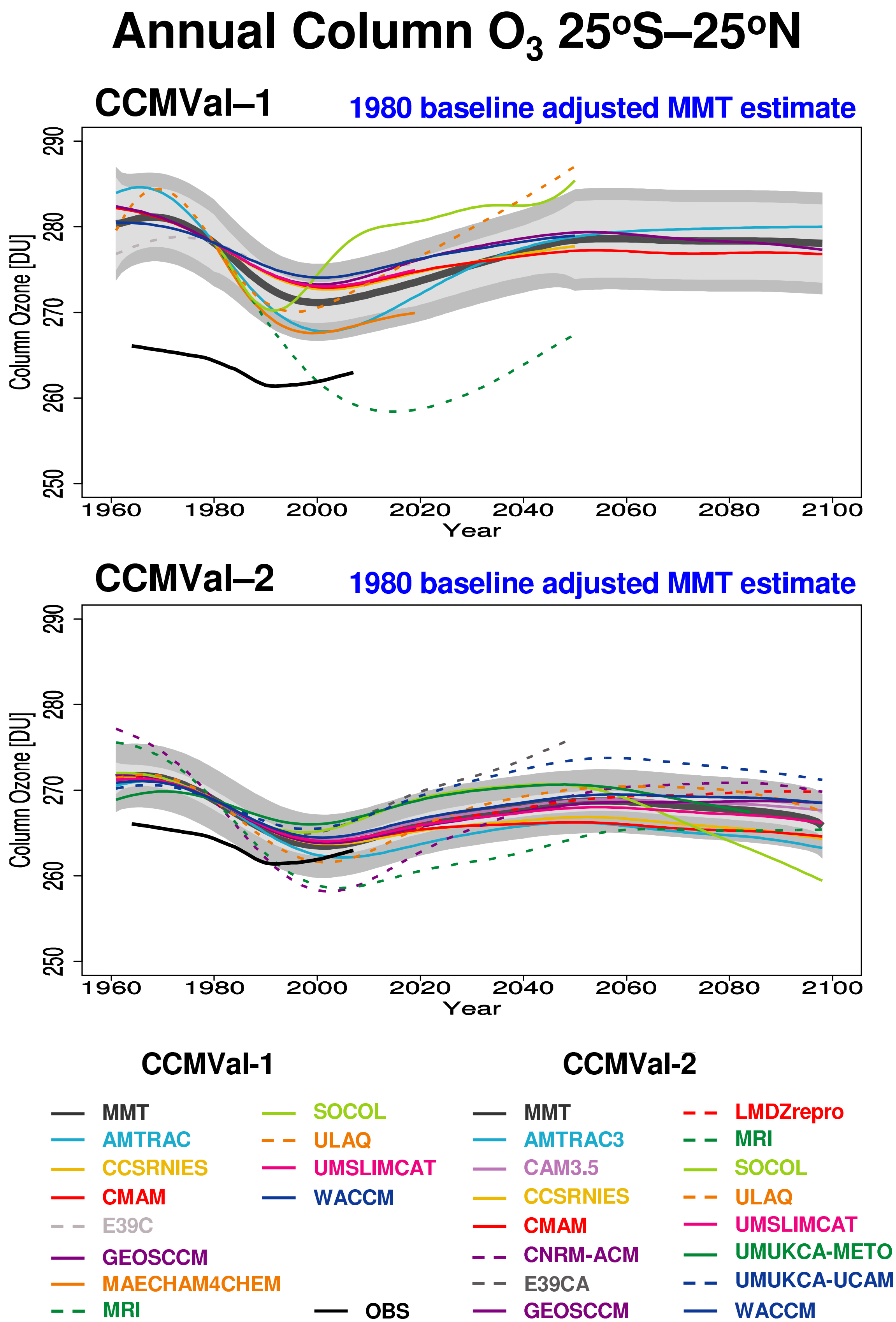

Figure 9S.2: 1980 baseline-adjusted multi-model trend (MMT) estimates of annually averaged Column O_3 (25°S-25°N) (heavy dark grey line) with 95% confidence and 95% prediction intervals appearing as light- and dark-grey shaded regions about the trend. The 1980 baseline-adjusted IMT estimates, and unadjusted lowess fit to the observations are additionally plotted. CCMVal-1 results appear in the upper panel and CCMVal-2 results appear in the lower panel.

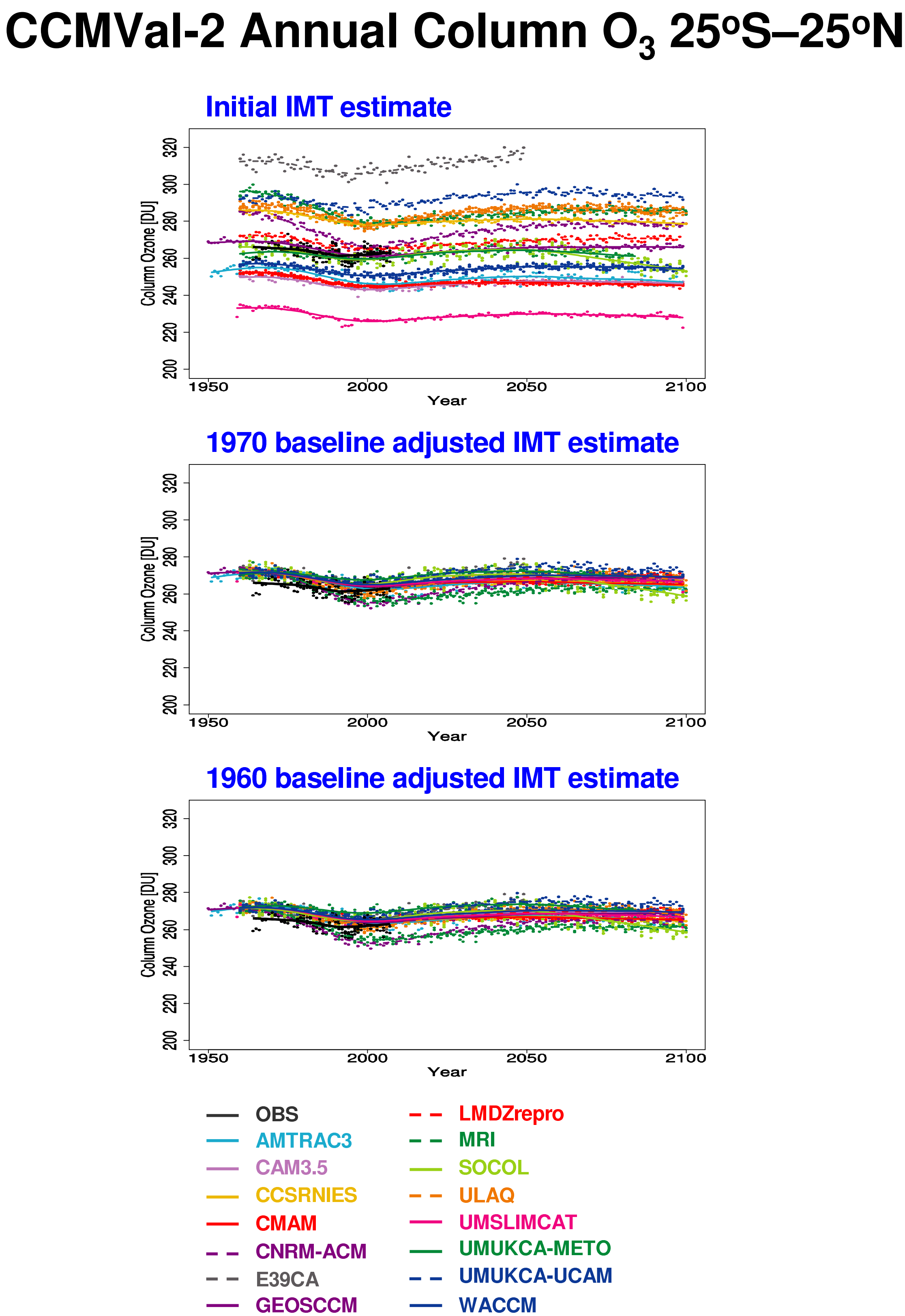

Figure 9S.3: Raw time series data of annually averaged Column O_3 (25°S-25°N) and initial IMT estimates (top panel), and 1970 (middle panel) and 1960 (bottom panel) baseline-adjusted time series data and baseline-adjusted IMT estimates for the TSAM analysis of CCMVal-2. Following Fig. 9S.1 a lowess fit to the observations appears as a black line in all panels and the observations are not baseline-adjusted.

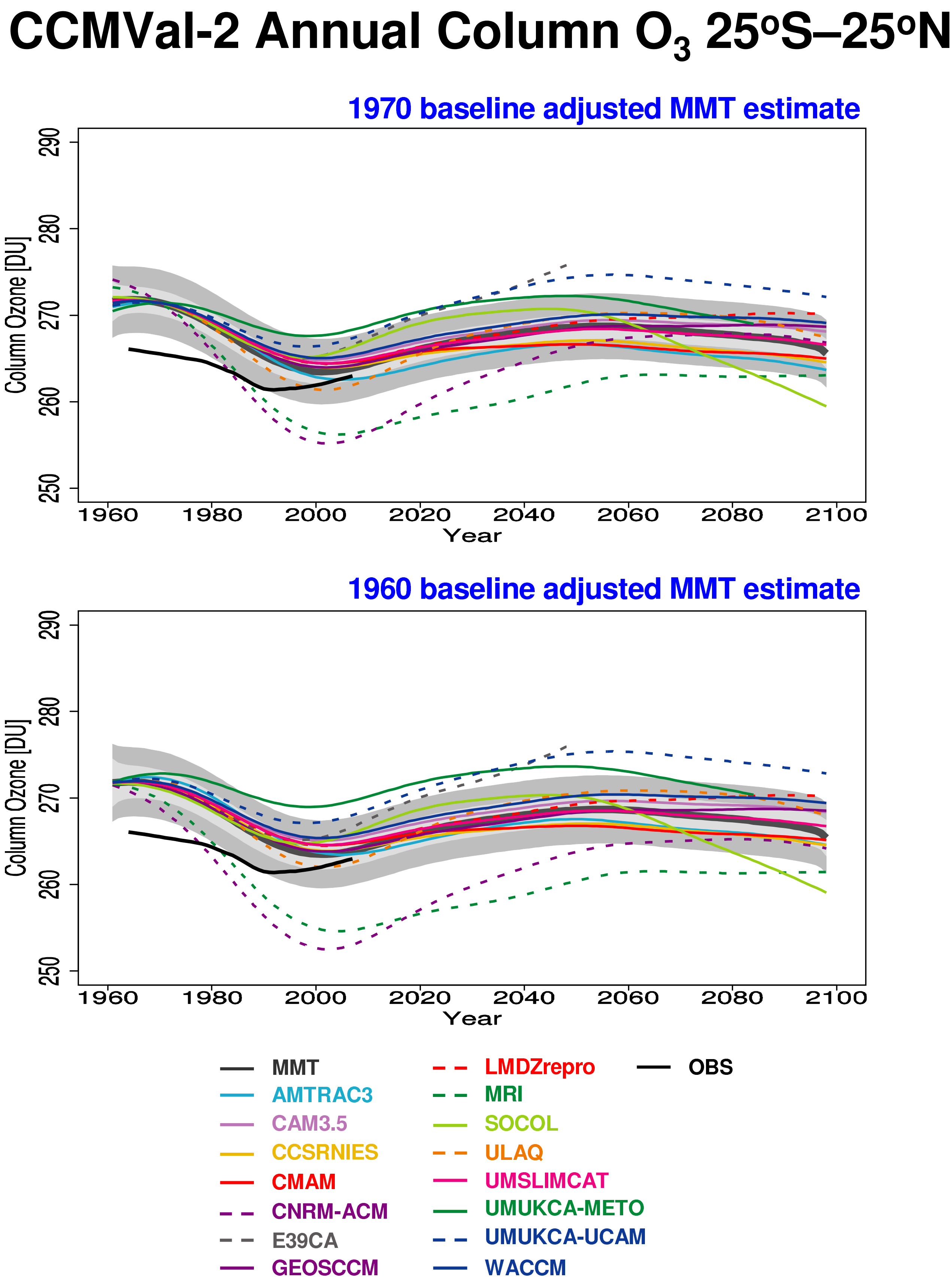

Figure 9S.4: CCMVal-2 1970 (top) and 1960 (bottom) baseline-adjusted IMT and MMT estimates of annually averaged Column O_3 (25°S-25°N) following Fig. 9S.2.

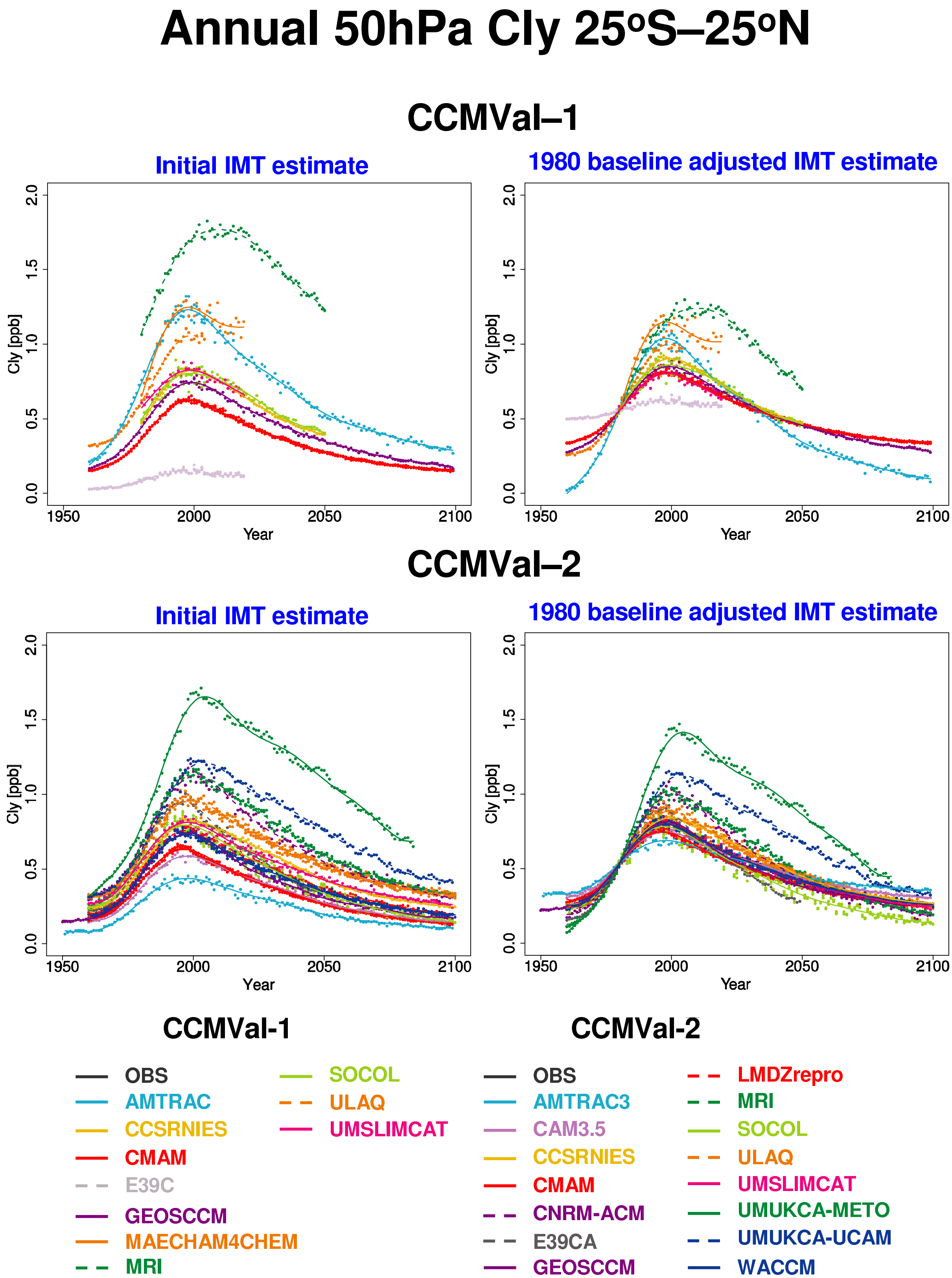

Figure 9S.5: As in Fig. 9S.1 but for 50hPa total inorganic chlorine (Cl_y) simulated by the models for the latitude range 25°S-25°N.

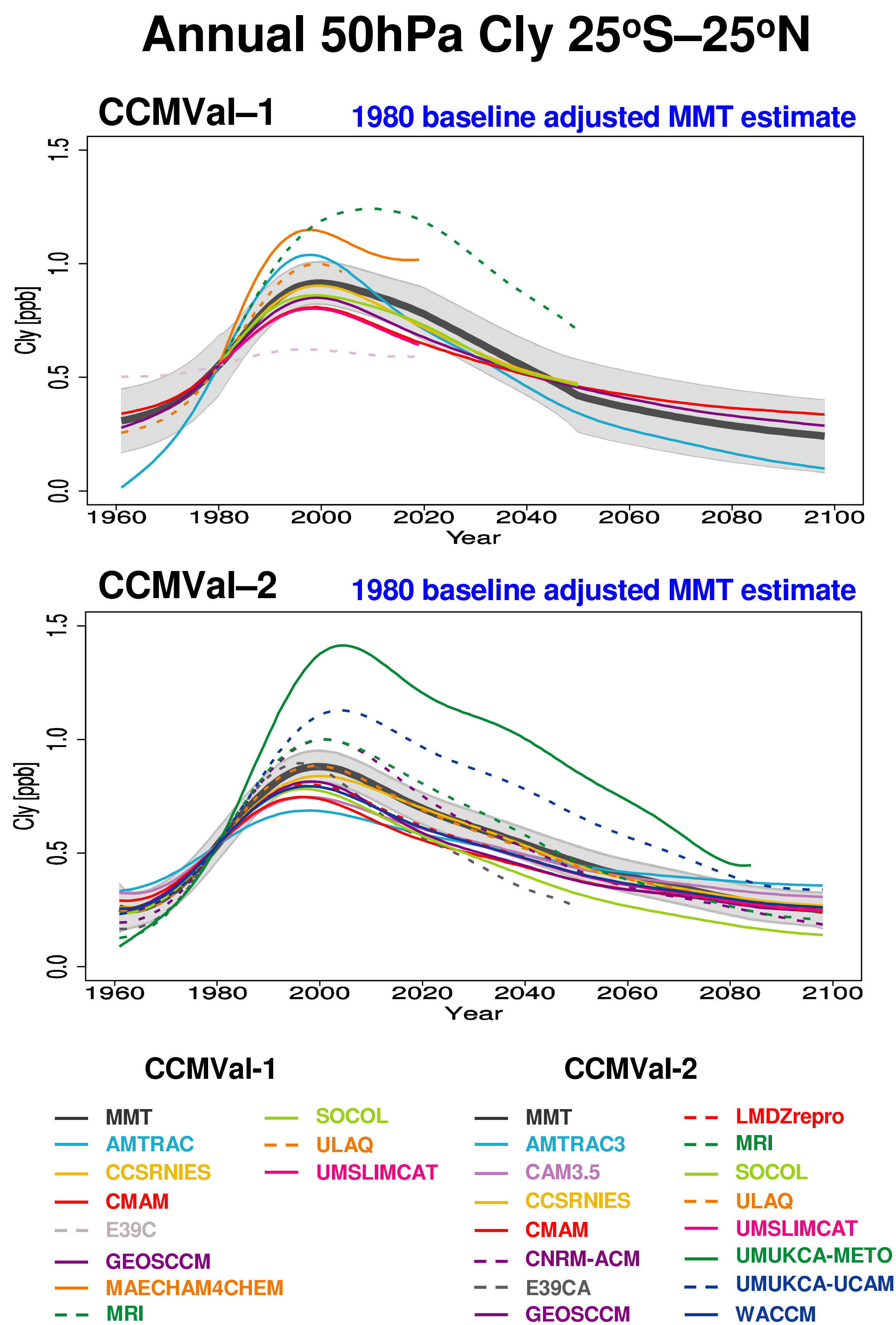

Figure 9S.6: As in Fig. 9S.2 but for 50hPa total inorganic chlorine (Cl_y) simulated by the models for the latitude range 25°S-25°N.

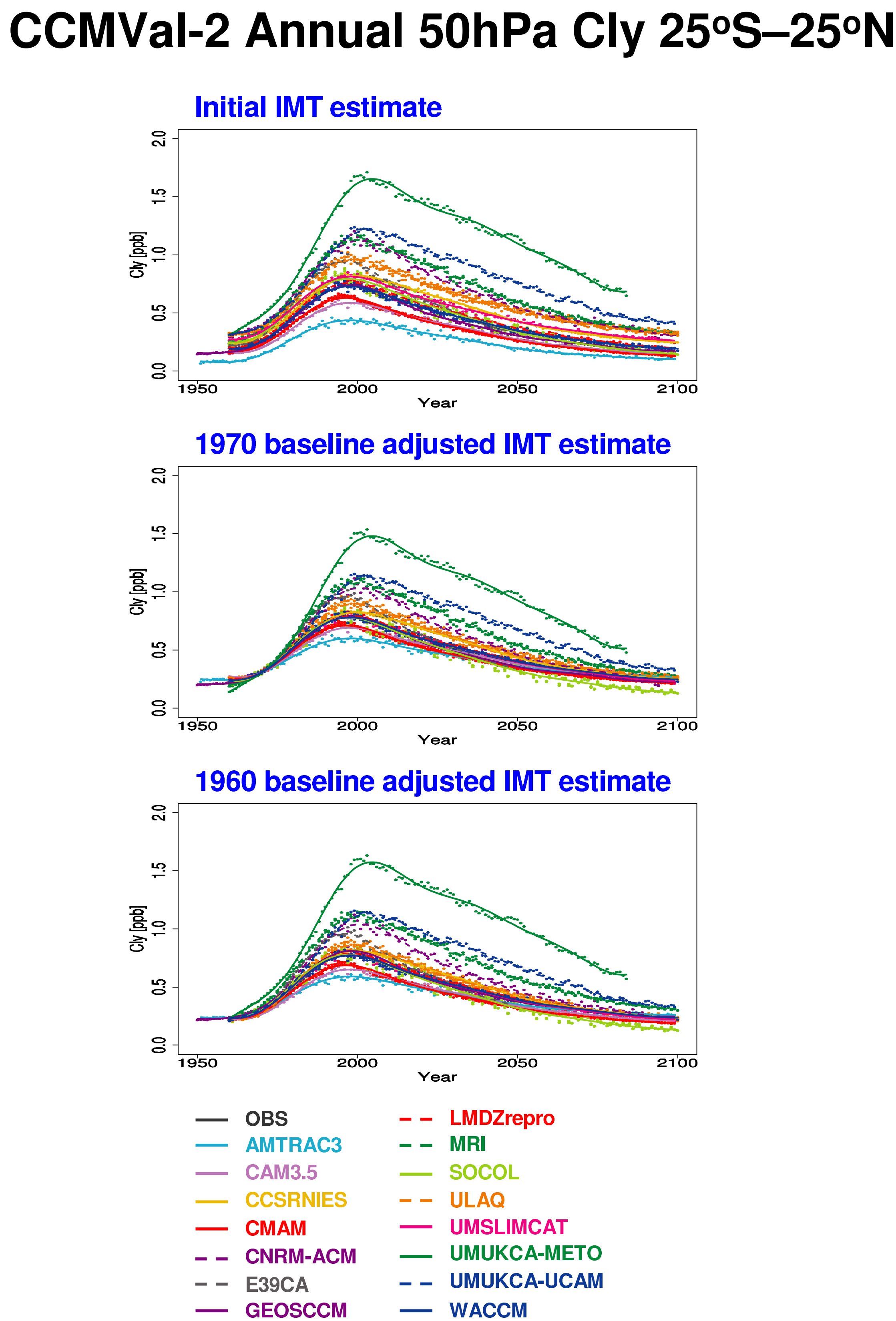

Figure 9S.7: As in Fig. 9S.3 but for 50hPa total inorganic chlorine (Cl_y) simulated by the models for the latitude range 25°S-25°N.

CCMVal-2 Annual 50hPa Cly 25°S–25°N

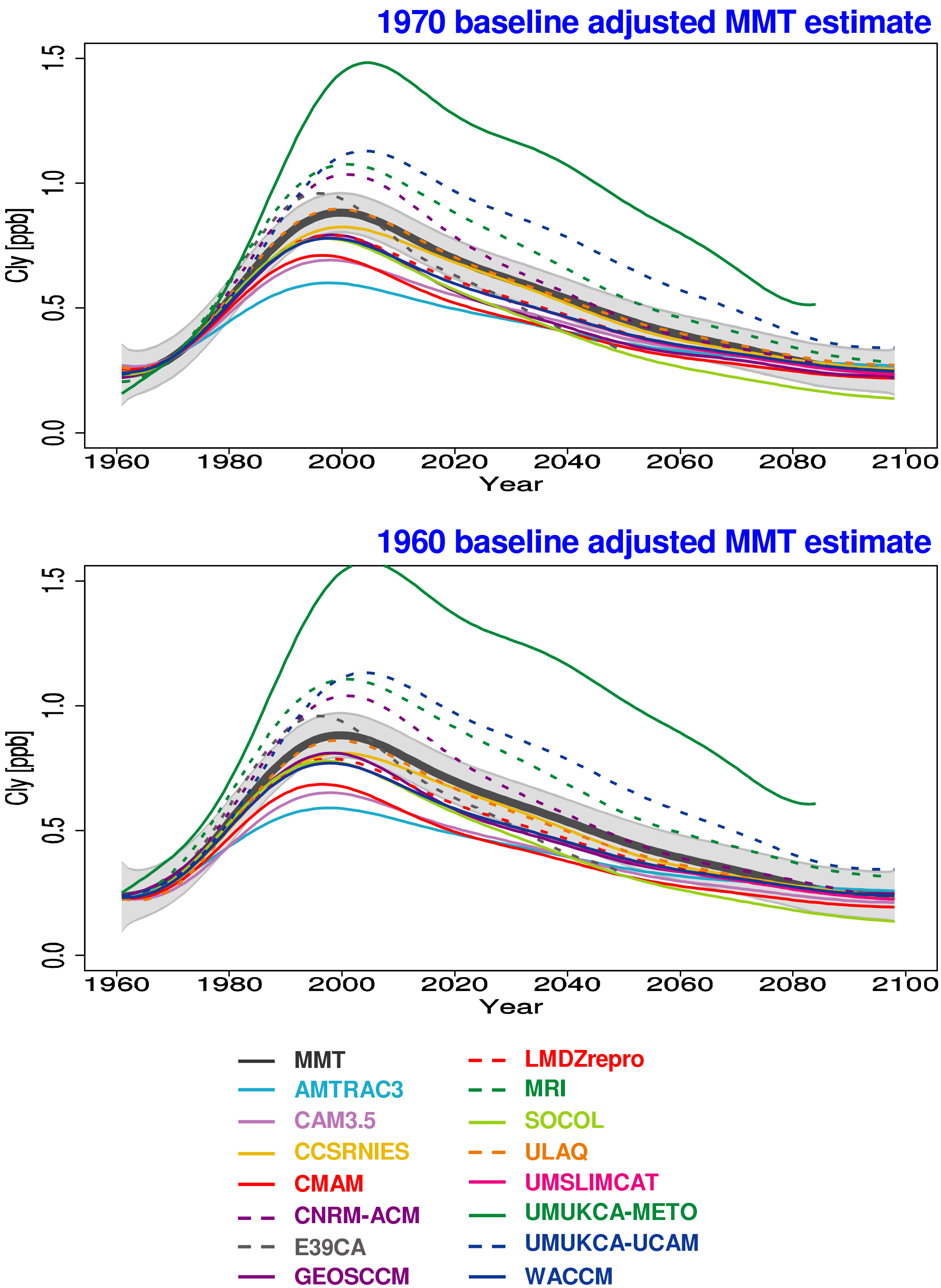

Figure 9S.8: As in Fig. 9S.4 but for 50hPa total inorganic chlorine (Cl_y) simulated by the models for the latitude range 25°S-25°N.

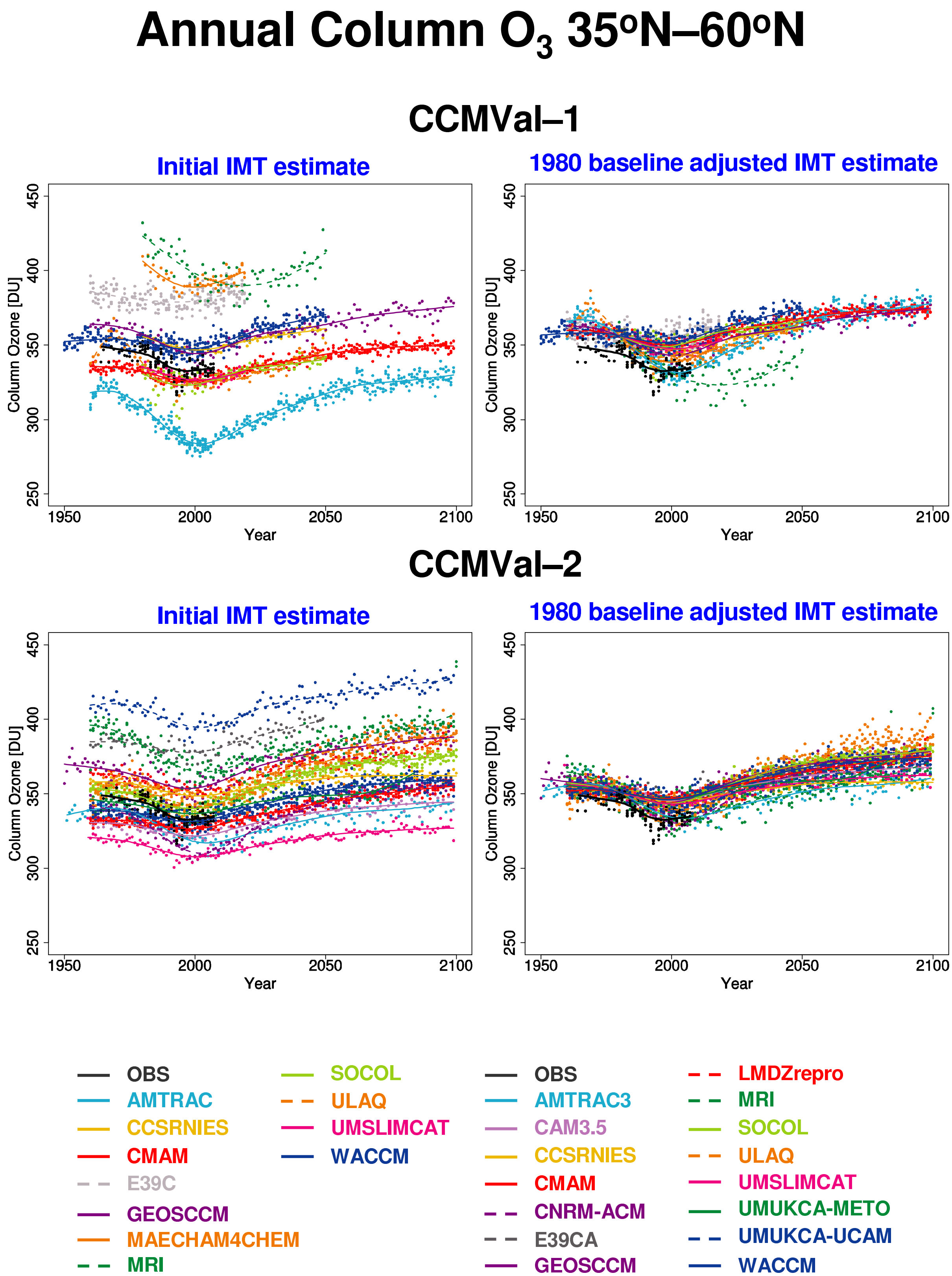

Figure 9S.9: As in Fig. 9S.1 but for the latitude range 35°N-60°N.

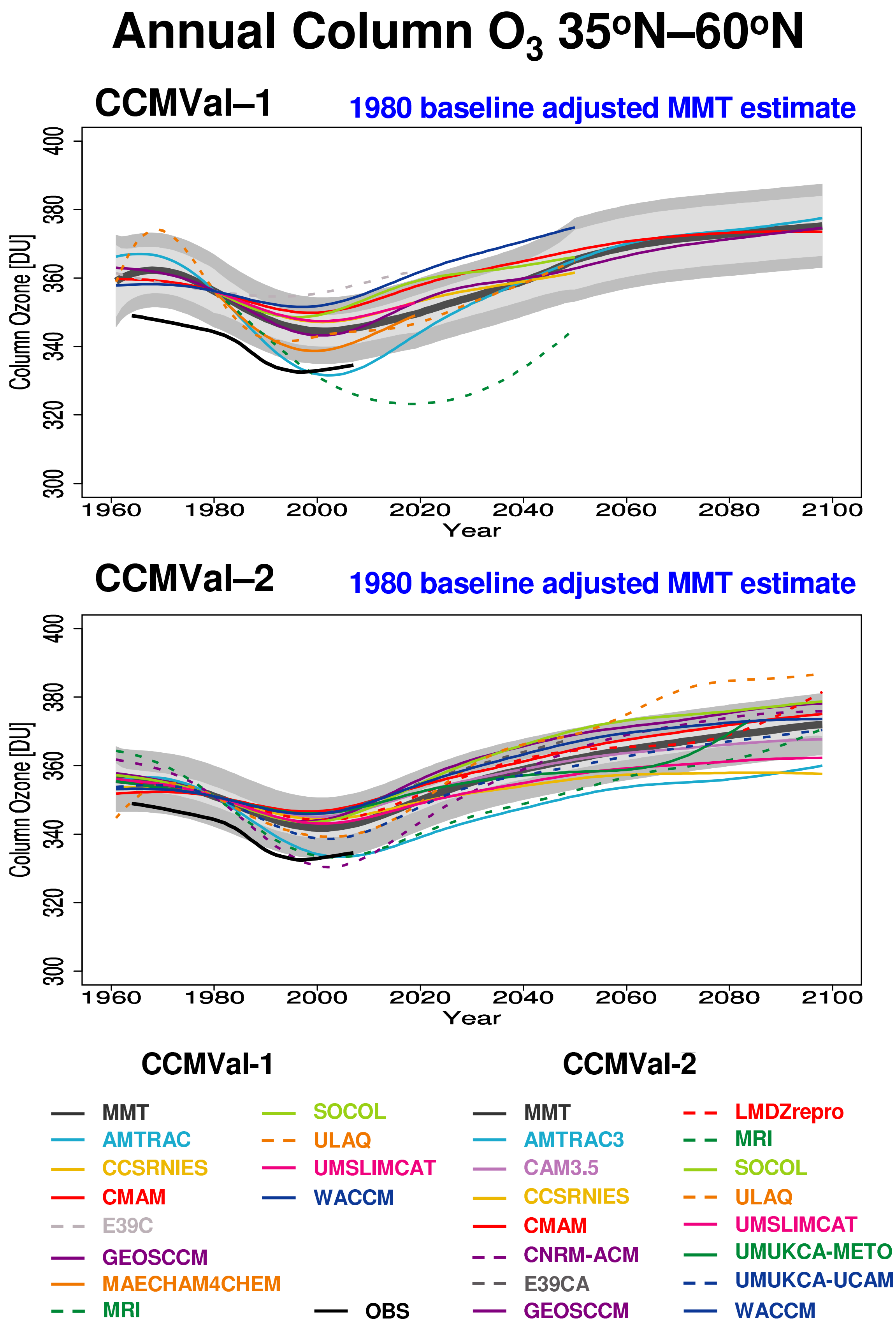

Figure 9S.10: As in Fig. 9S.2 but for the latitude range 35°N-60°N.

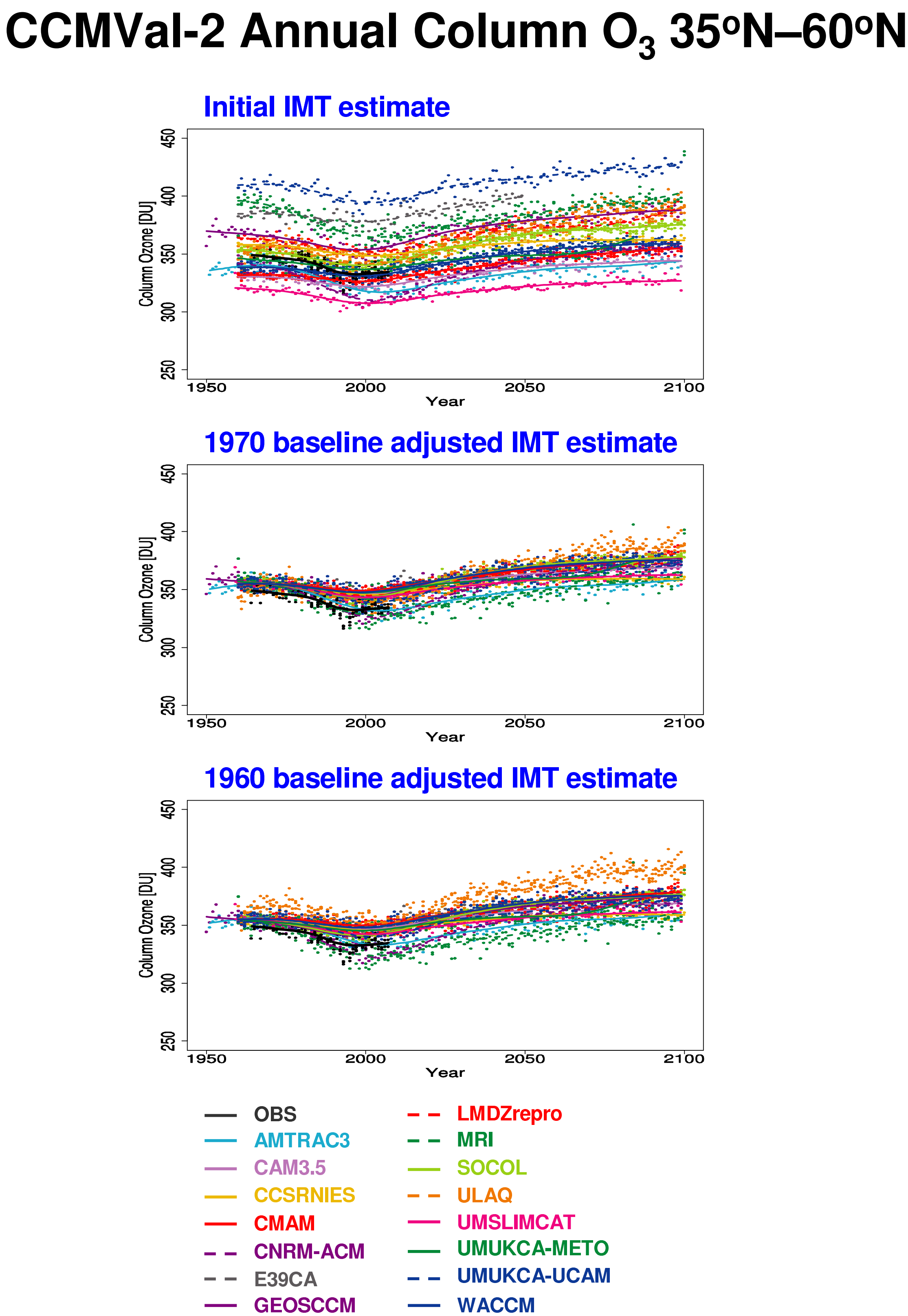

Figure 9S.11: As in Fig. 9S.3 but for the latitude range 35°N-60°N.

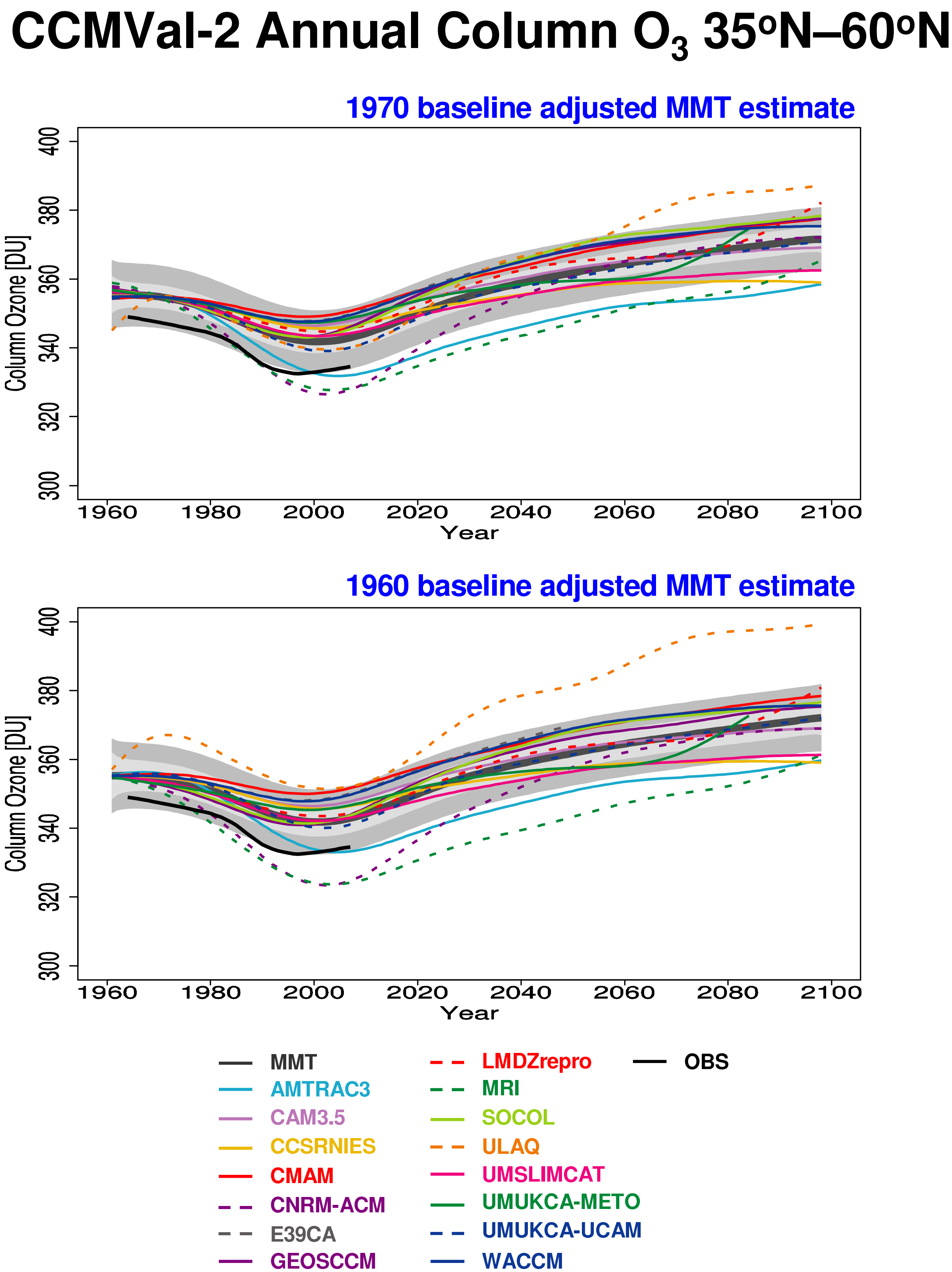

Figure 9S.12: As in Fig. 9S.4 but for the latitude range 35°N-60°N.

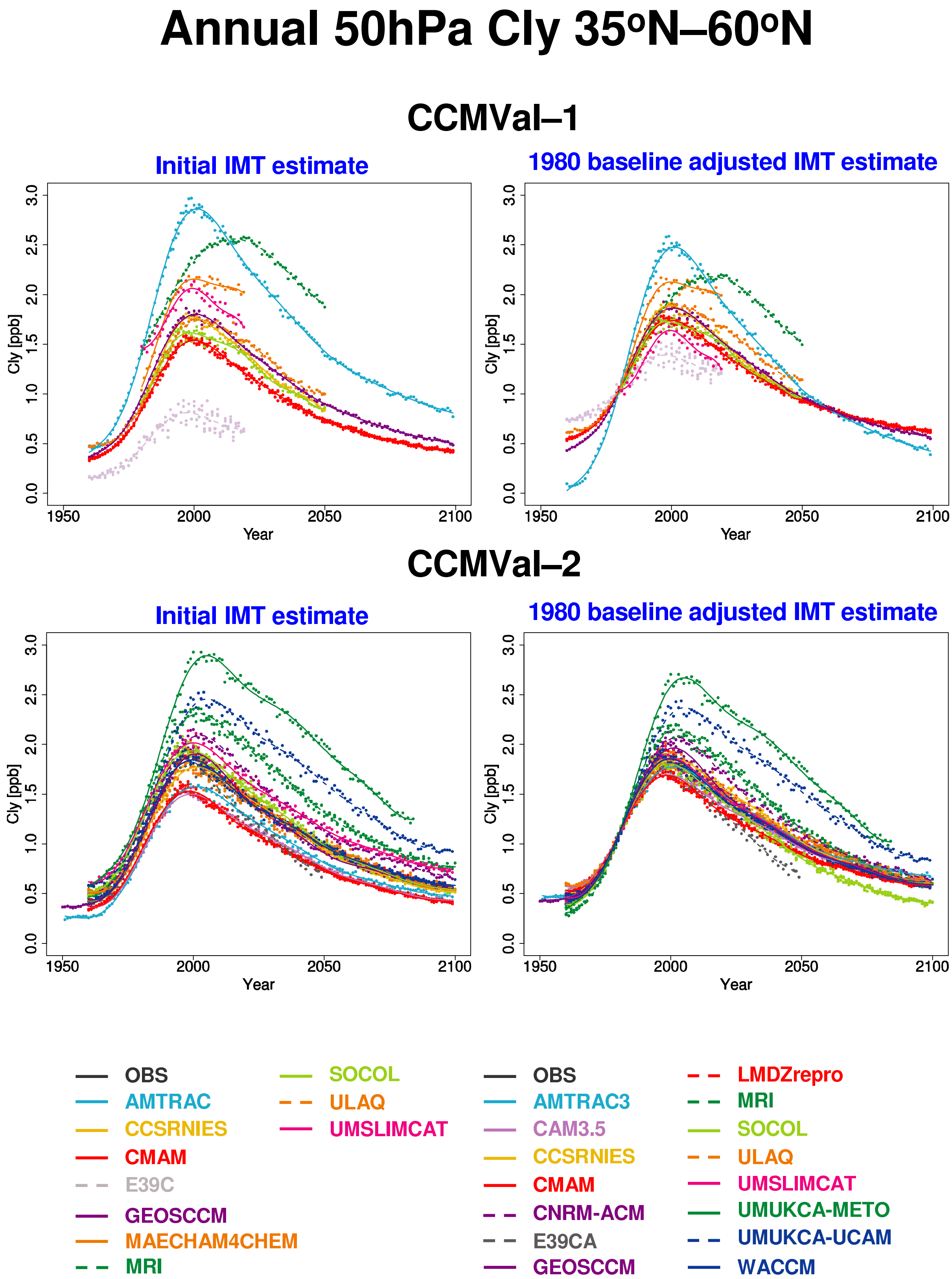

Figure 9S.13: As in Fig. 9S.5 but for the latitude range 35°N-60°N.

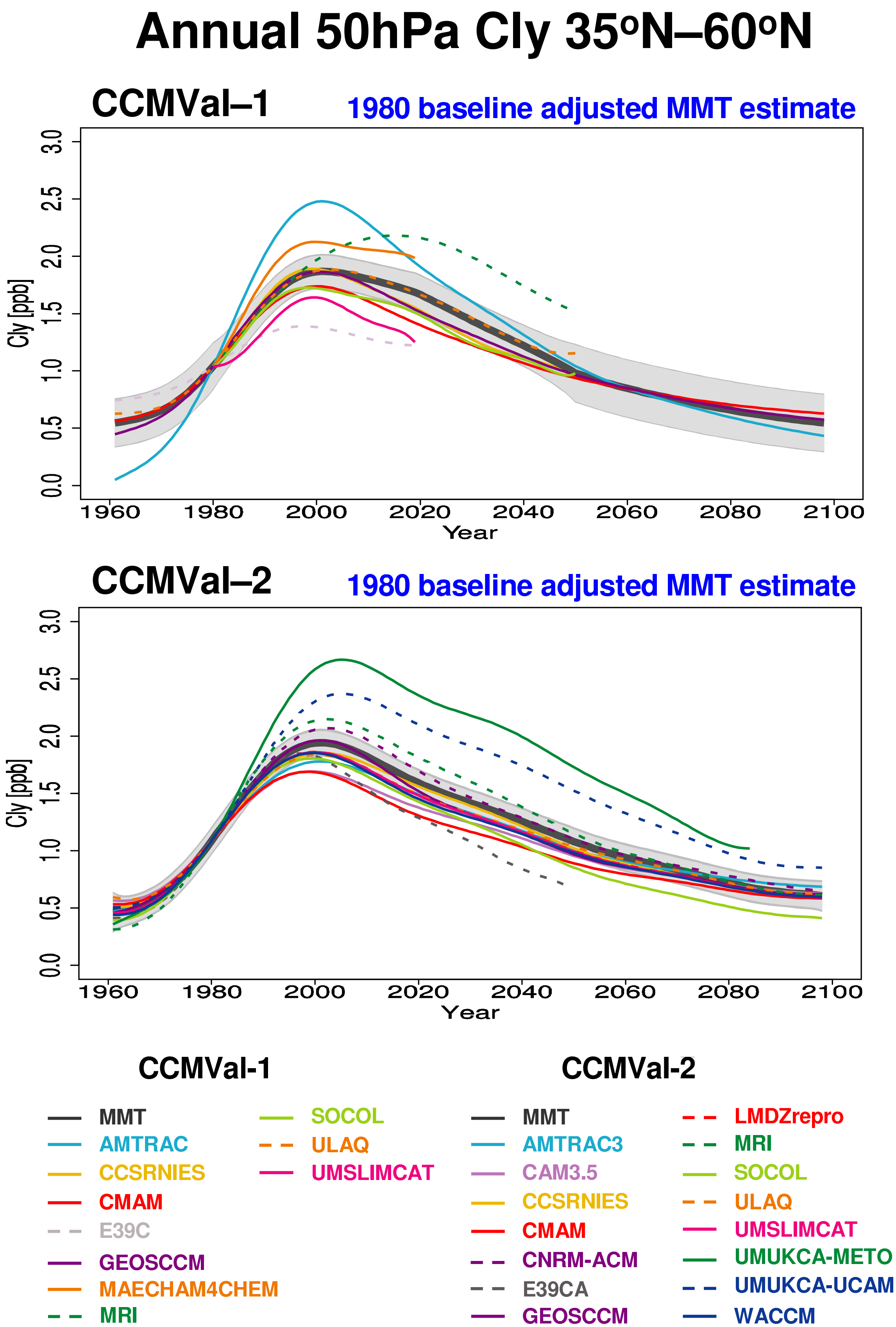

Figure 9S.14: As in Fig. 9S.6 but for the latitude range 35°N-60°N.

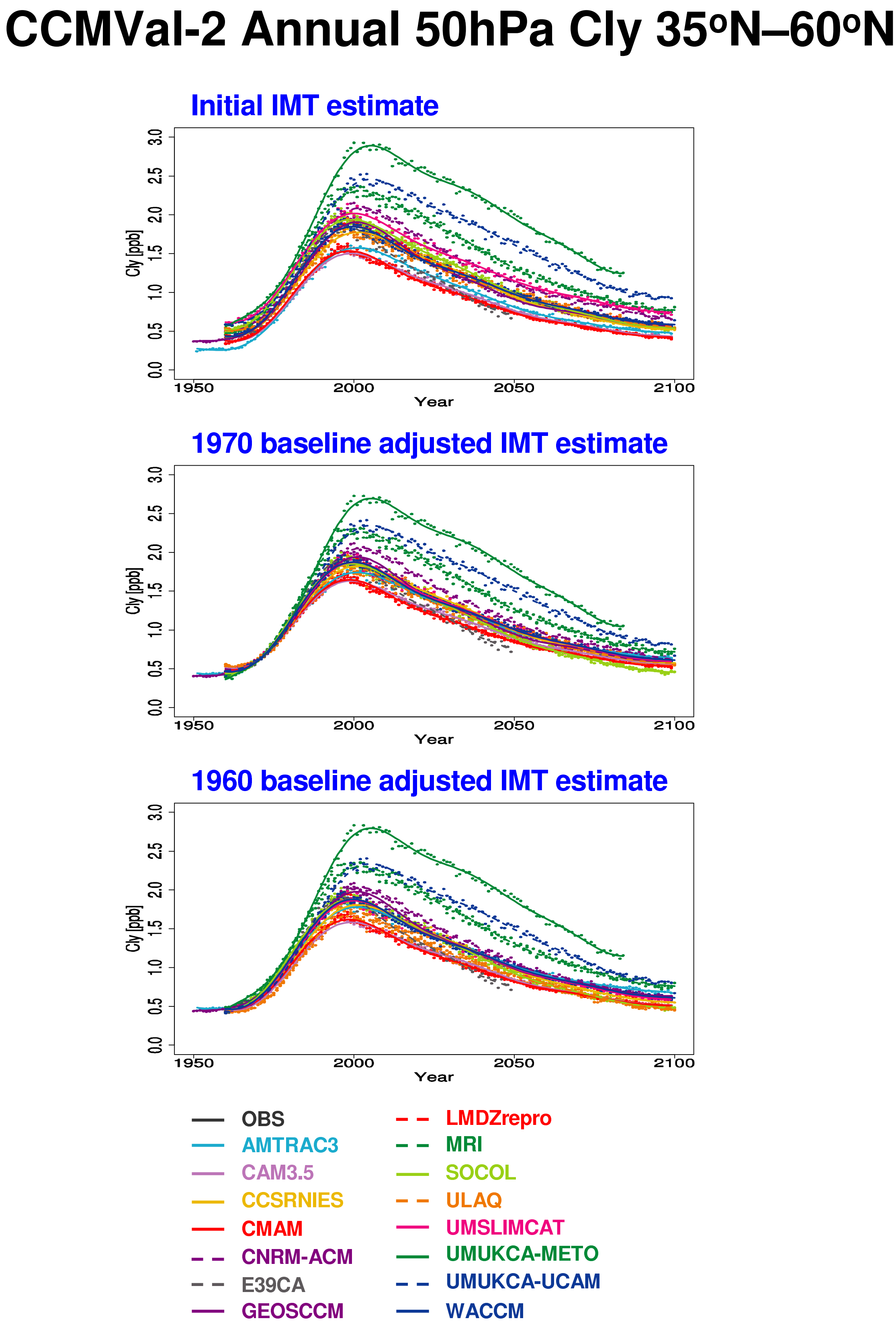

Figure 9S.15: As in Fig. 9S.7 but for the latitude range 35°N-60°N.

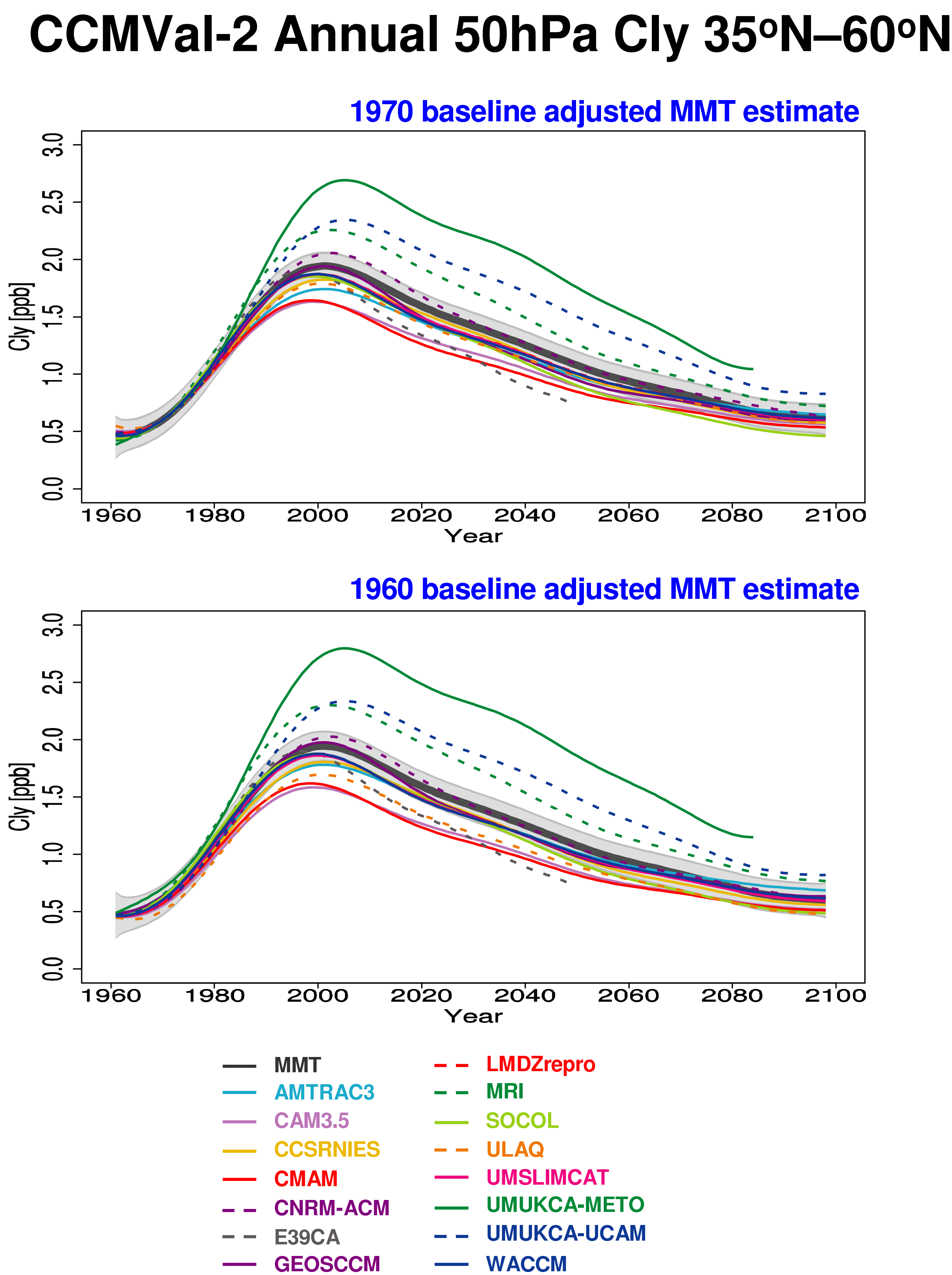

Figure 9S.16: As in Fig. 9S.8 but for the latitude range 35°N-60°N.

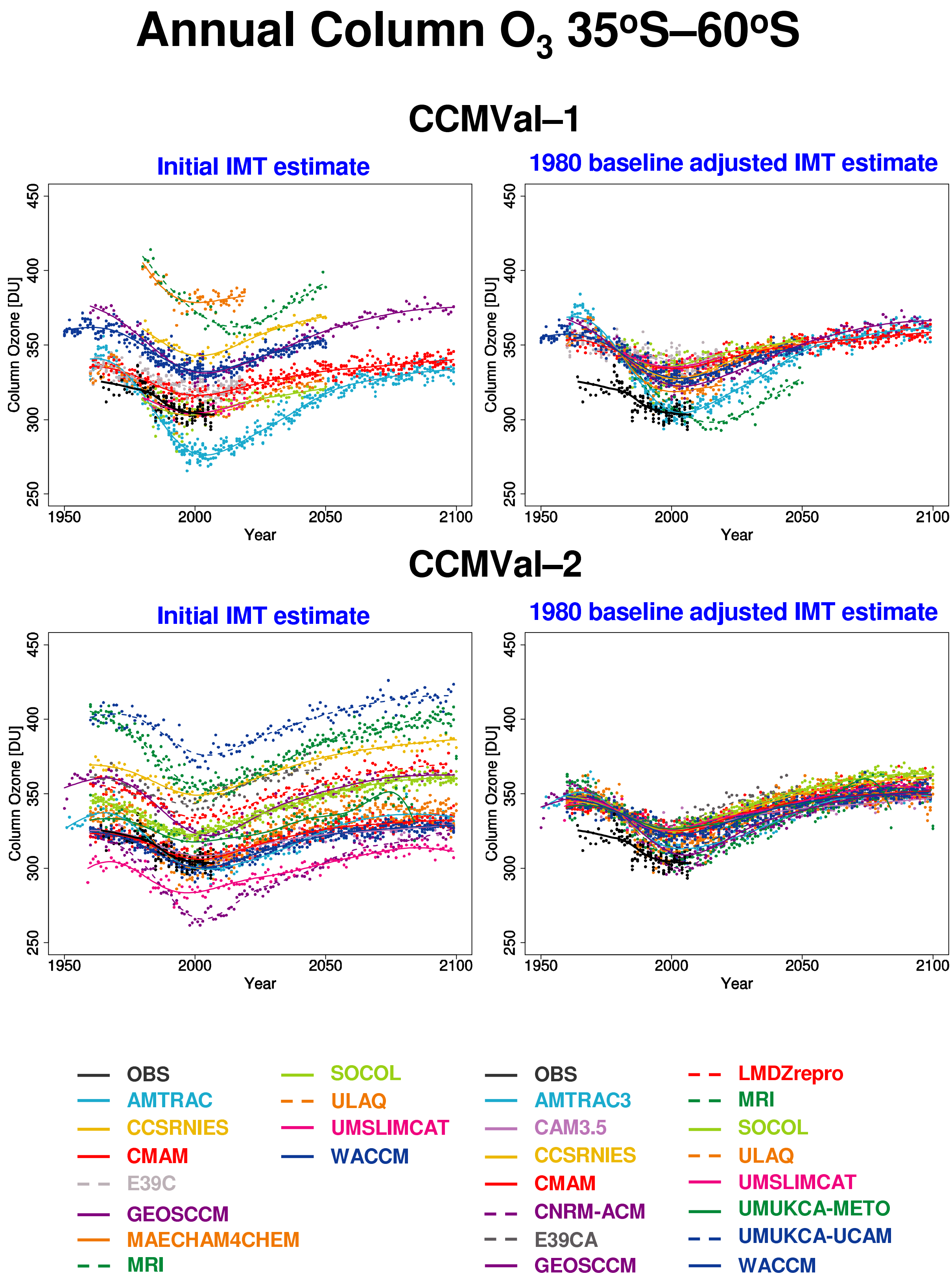

Figure 9S.17: As in Fig. 9S.1 but for the latitude range 35°S-60°S.

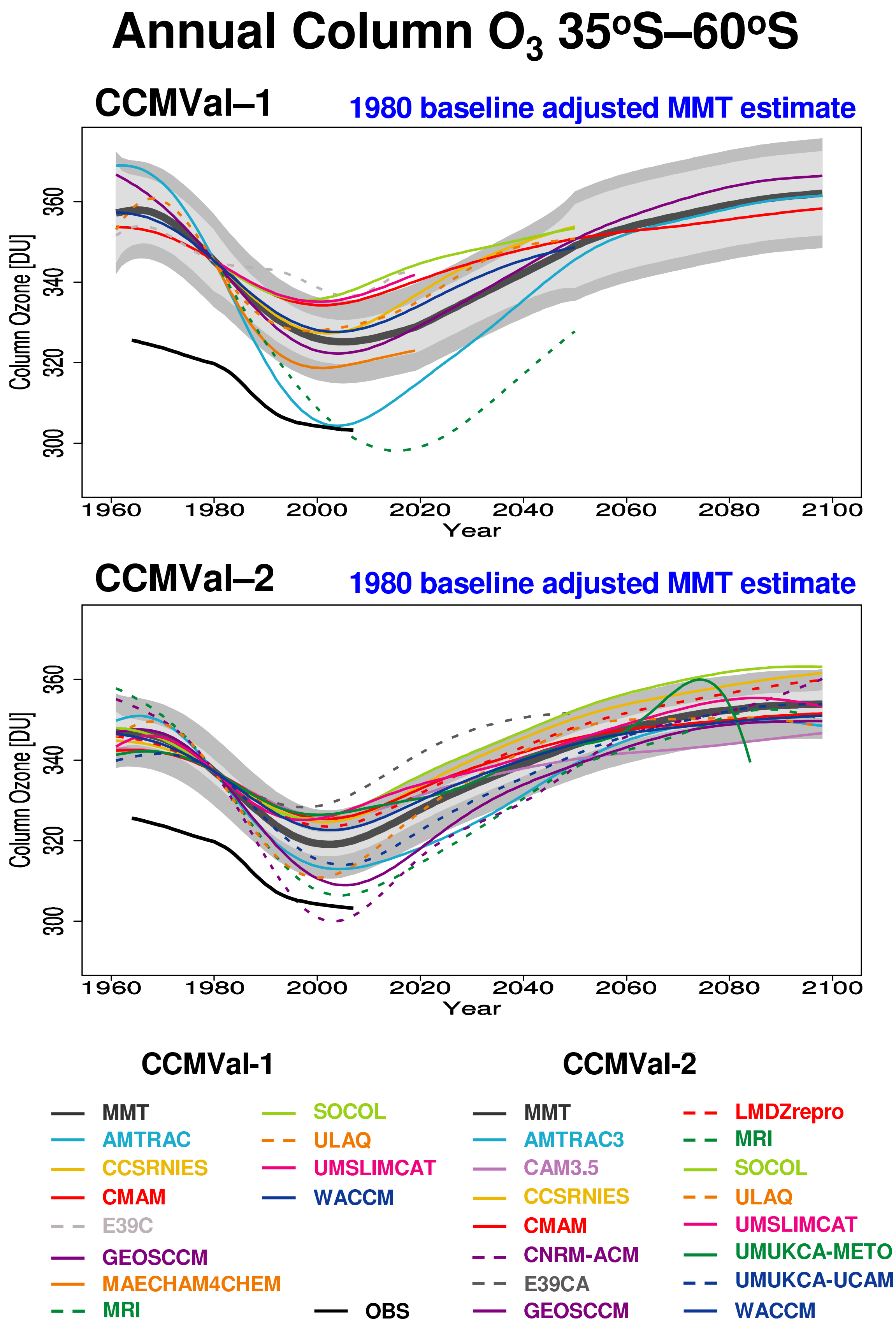

Figure 9S.18: As in Fig. 9S.2 but for the latitude range 35°S-60°S.

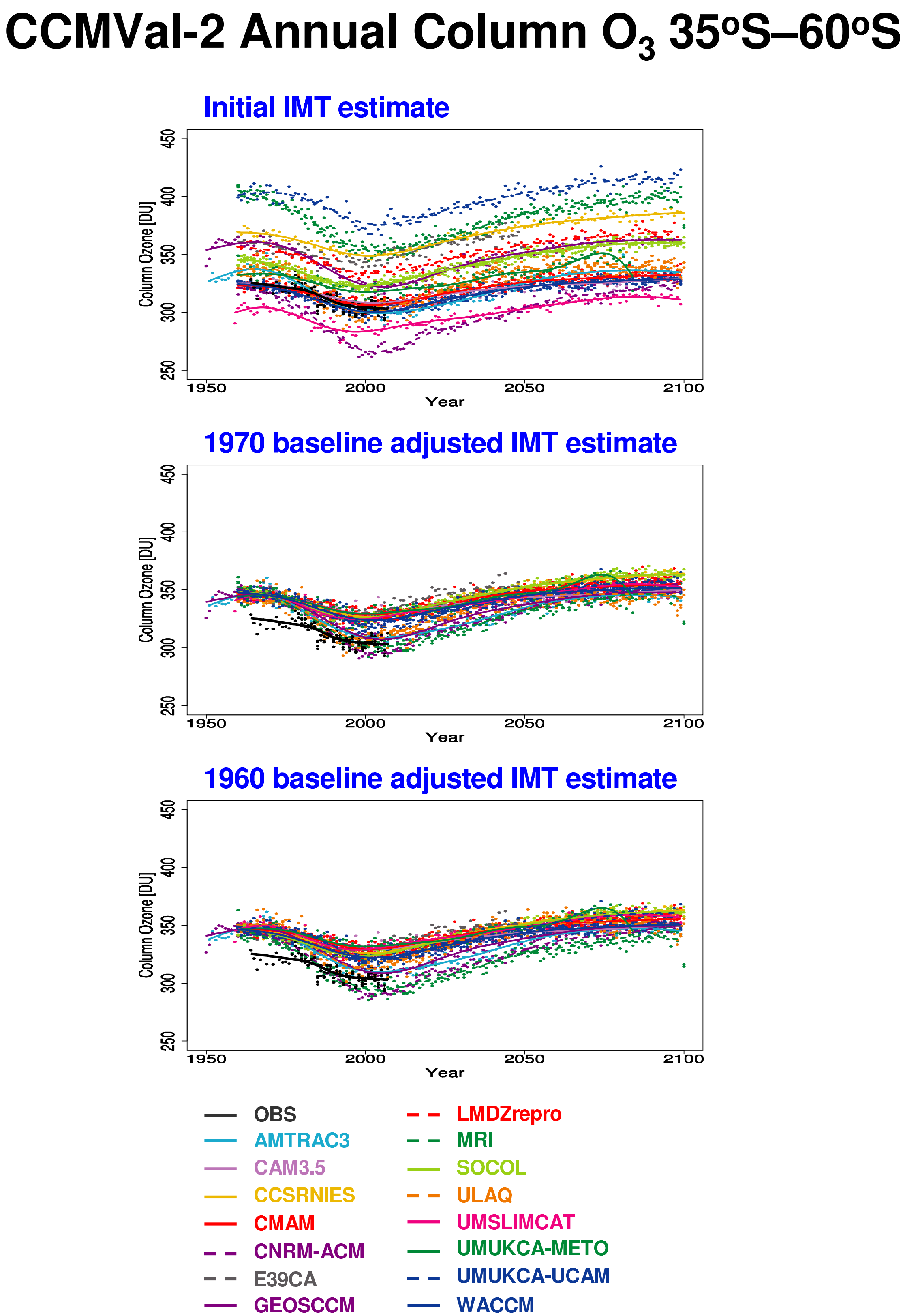

Figure 9S.19: As in Fig. 9S.3 but for the latitude range 35°S-60°S.

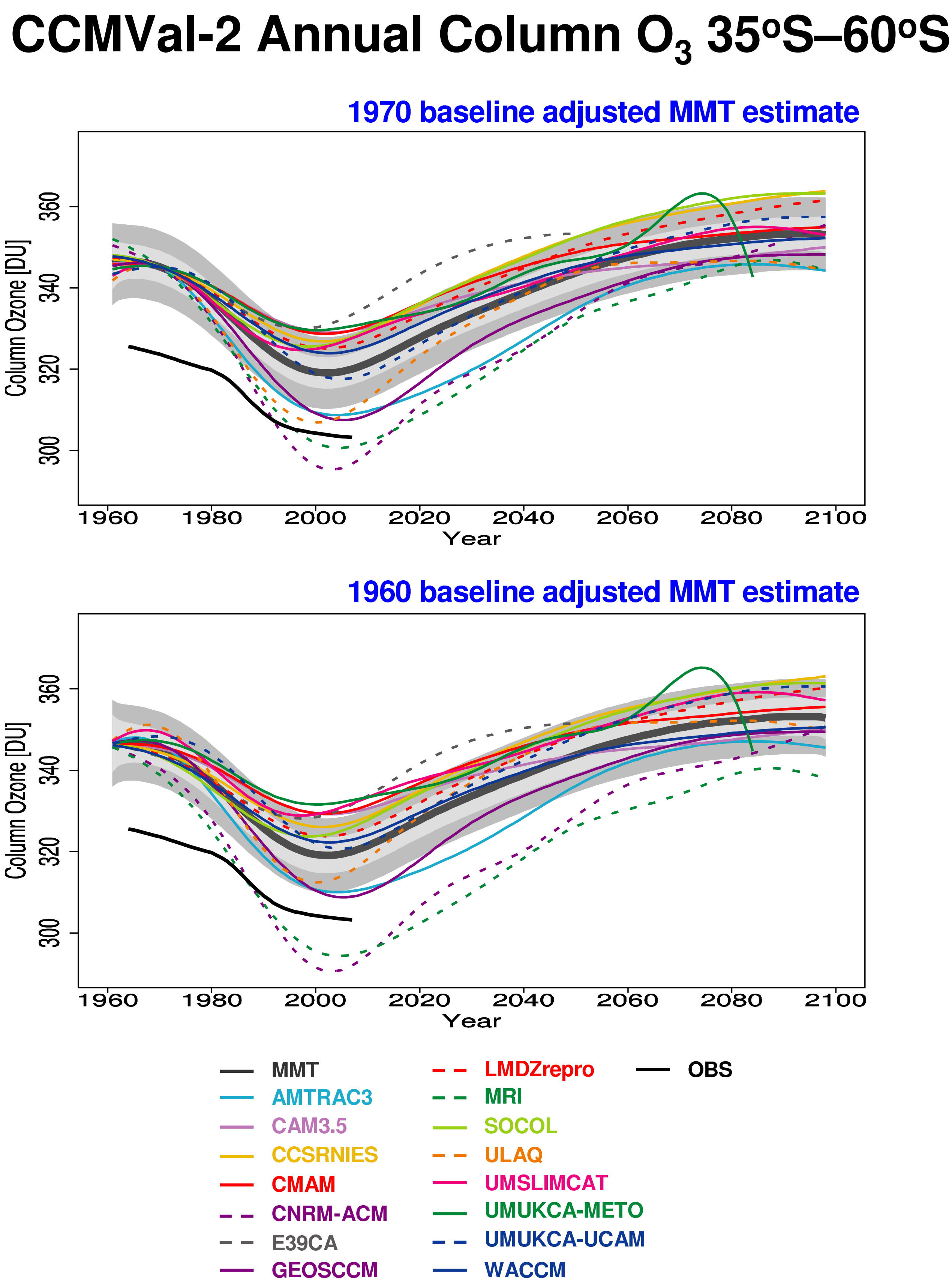

Figure 9S.20: As in Fig. 9S.4 but for the latitude range 35°S-60°S.

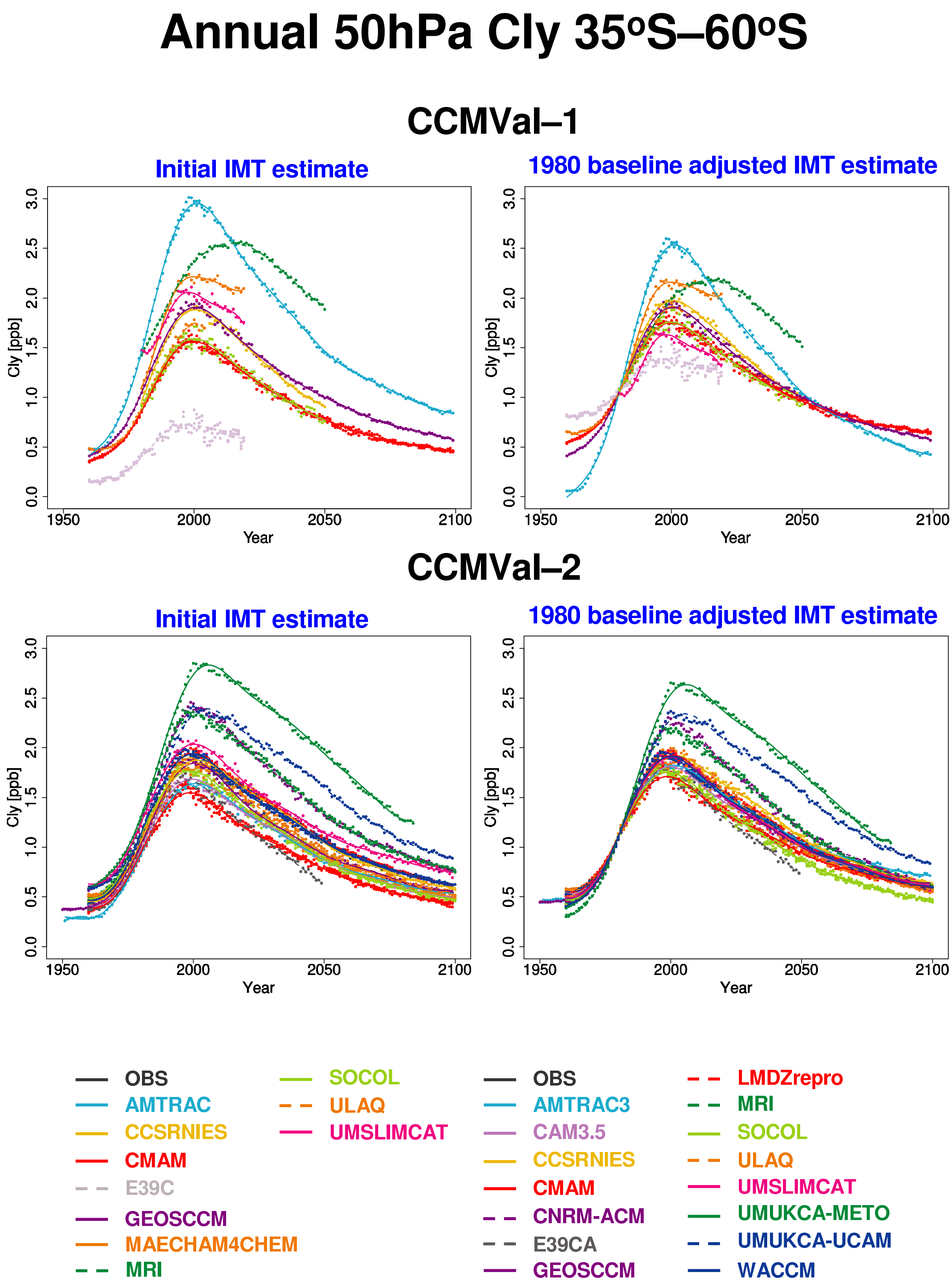

Figure 9S.21: As in Fig. 9S.5 but for the latitude range 35°S-60°S.

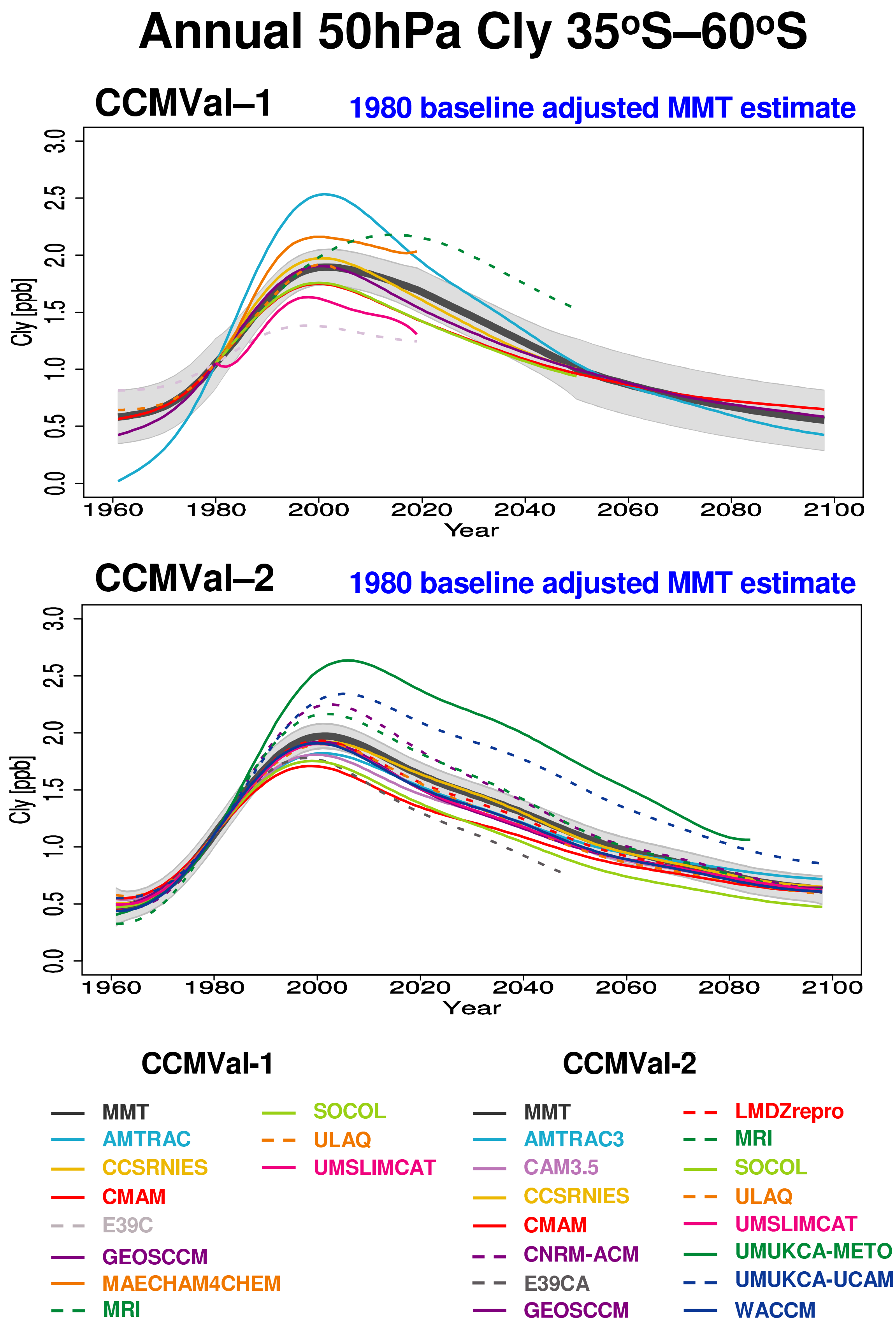

Figure 9S.22: As in Fig. 9S.6 but for the latitude range 35°S-60°S.

CCMVal-2 Annual 50hPa Cly 35ºS–60ºS

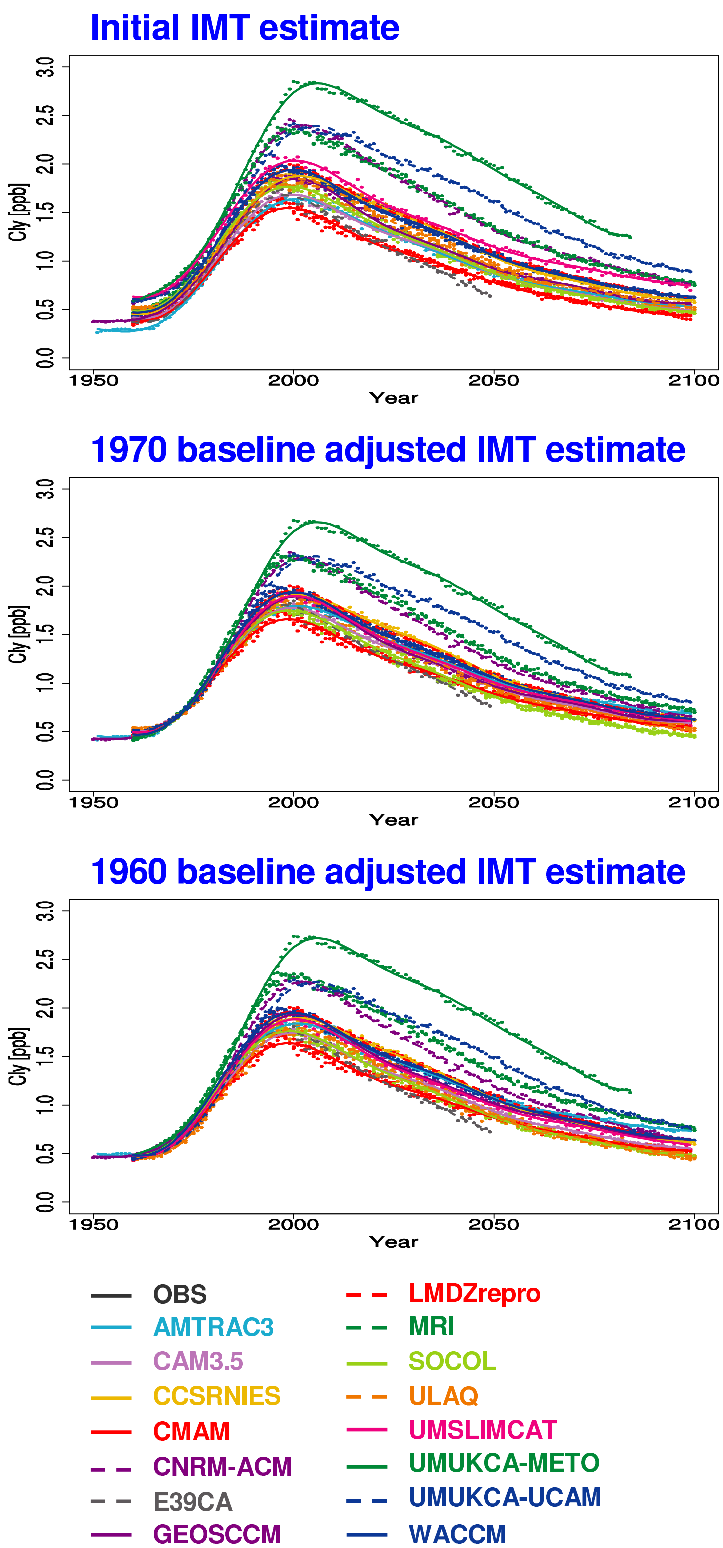

Figure 9S.23: As in Fig. 9S.7 but for the latitude range 35°S-60°S.

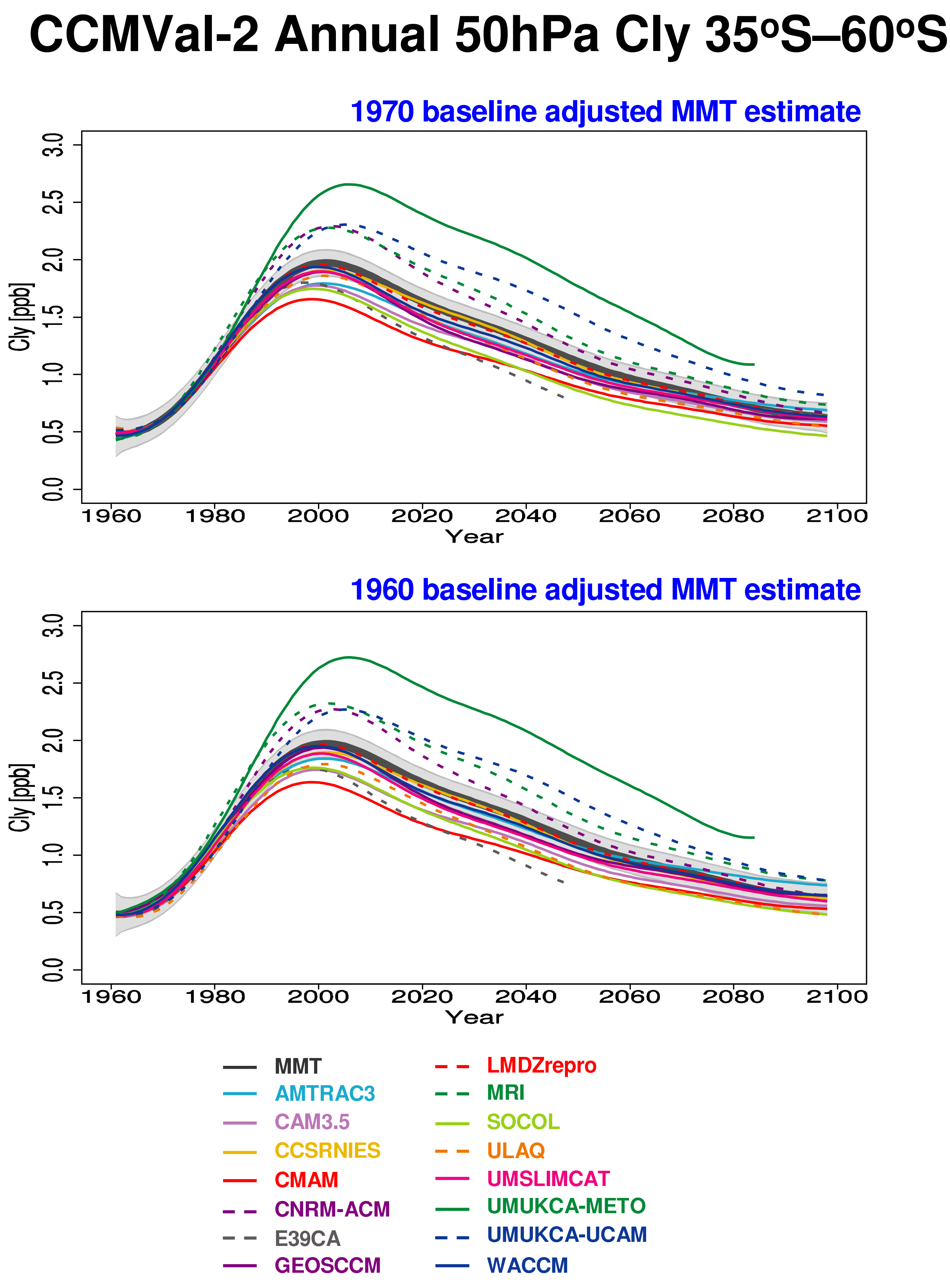

Figure 9S.24: As in Fig. 9S.8 but for the latitude range 35°S-60°S.

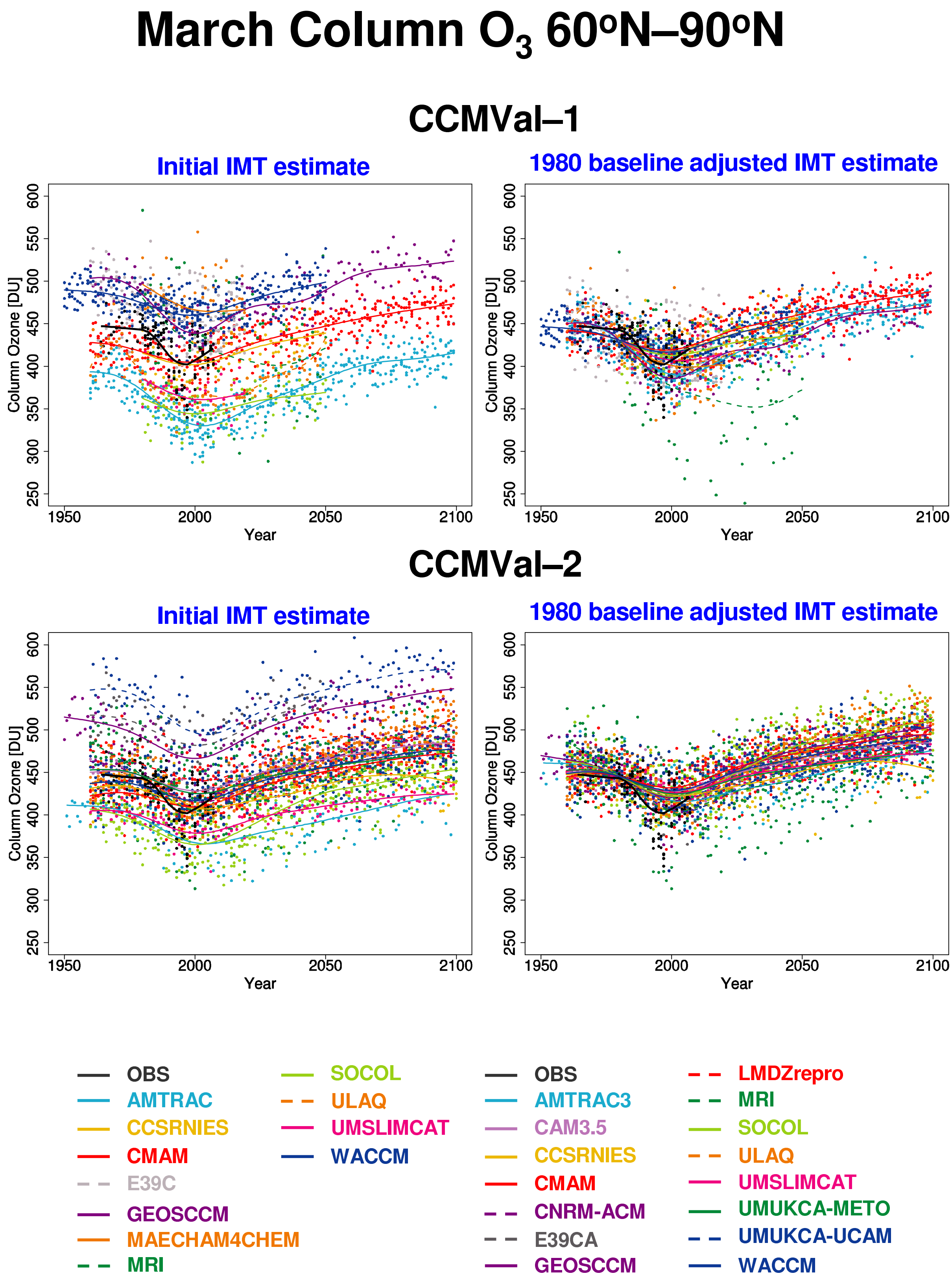

Figure 9S.25: As in Fig. 9S.1 but for the month of March and the latitude range 60°N-90°N.

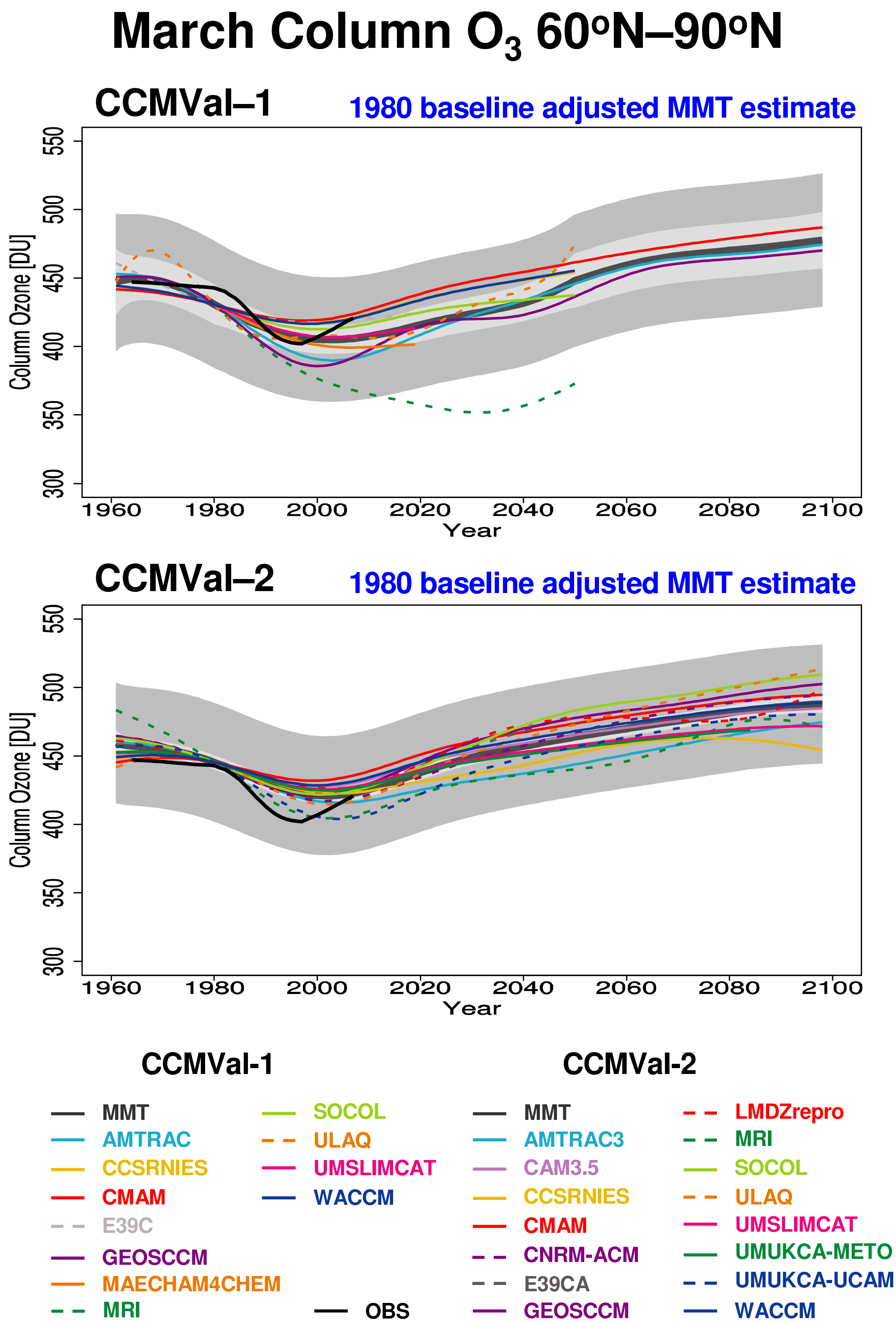

Figure 9S.26: As in Fig. 9S.2 but for the month of March and the latitude range 60°N-90°N.

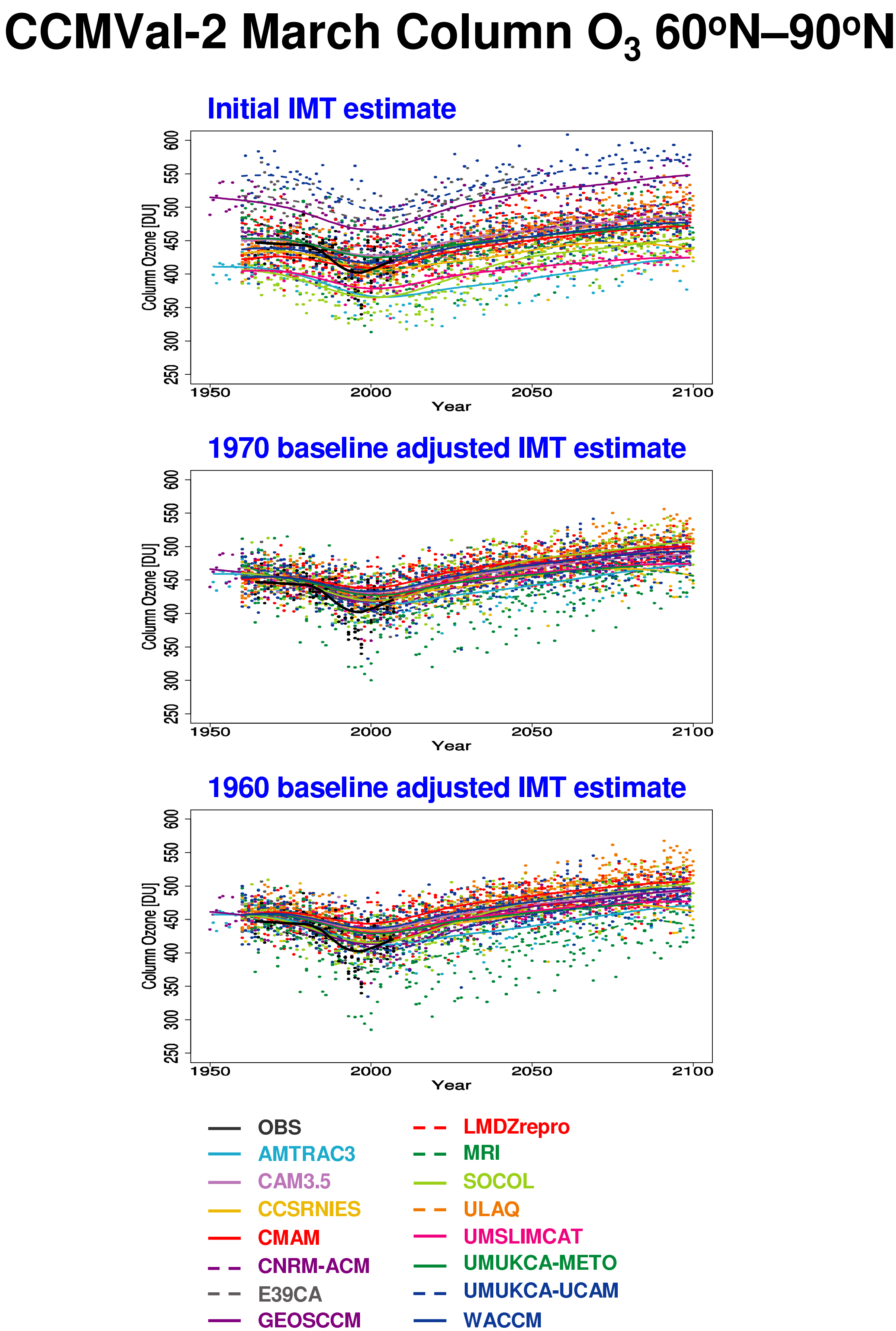

Figure 9S.27: As in Fig. 9S.3 but for the month of March and the latitude range 60°N-90°N.

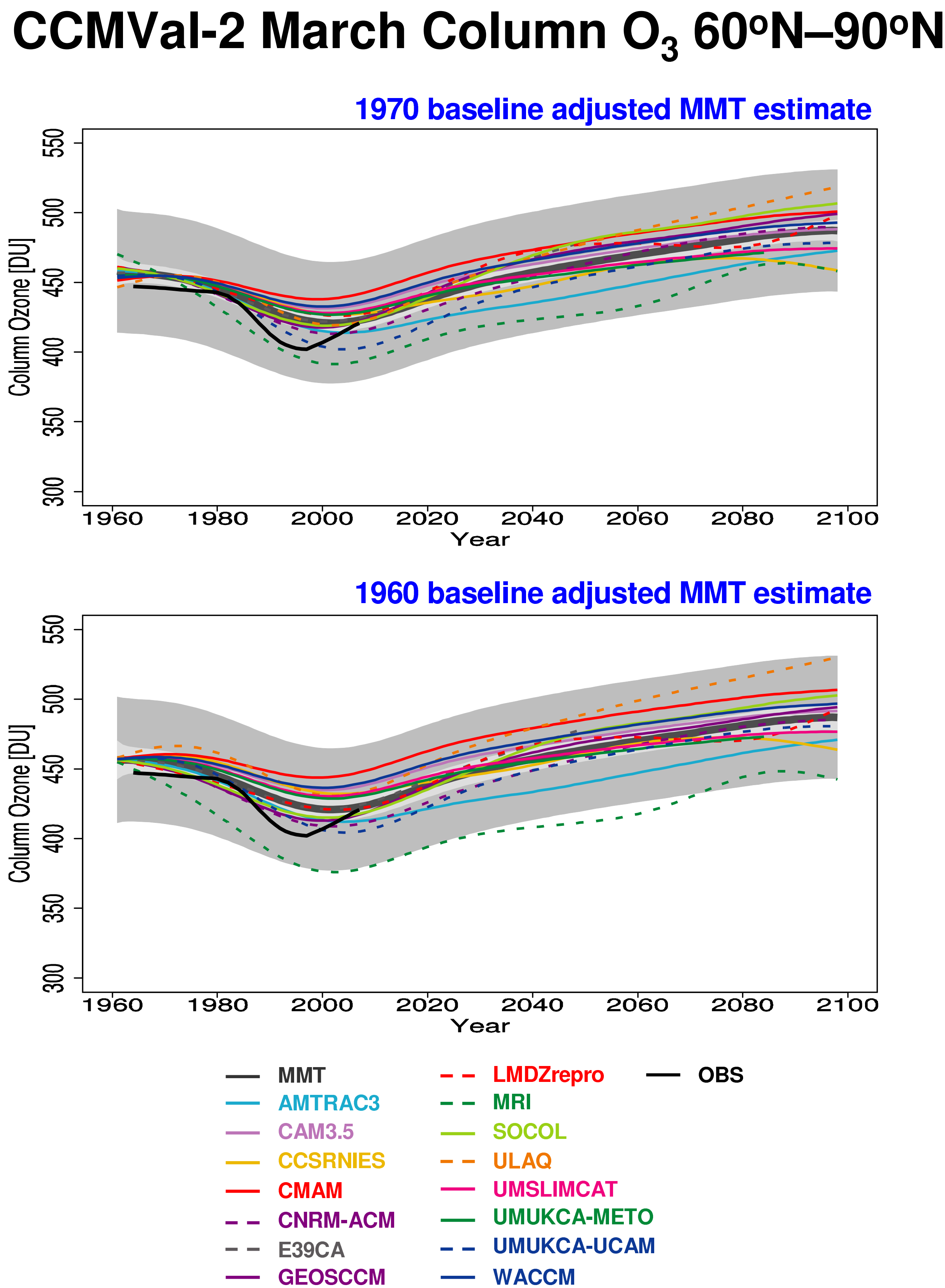

Figure 9S.28: As in Fig. 9S.4 but for the month of March and the latitude range 60°N-90°N.

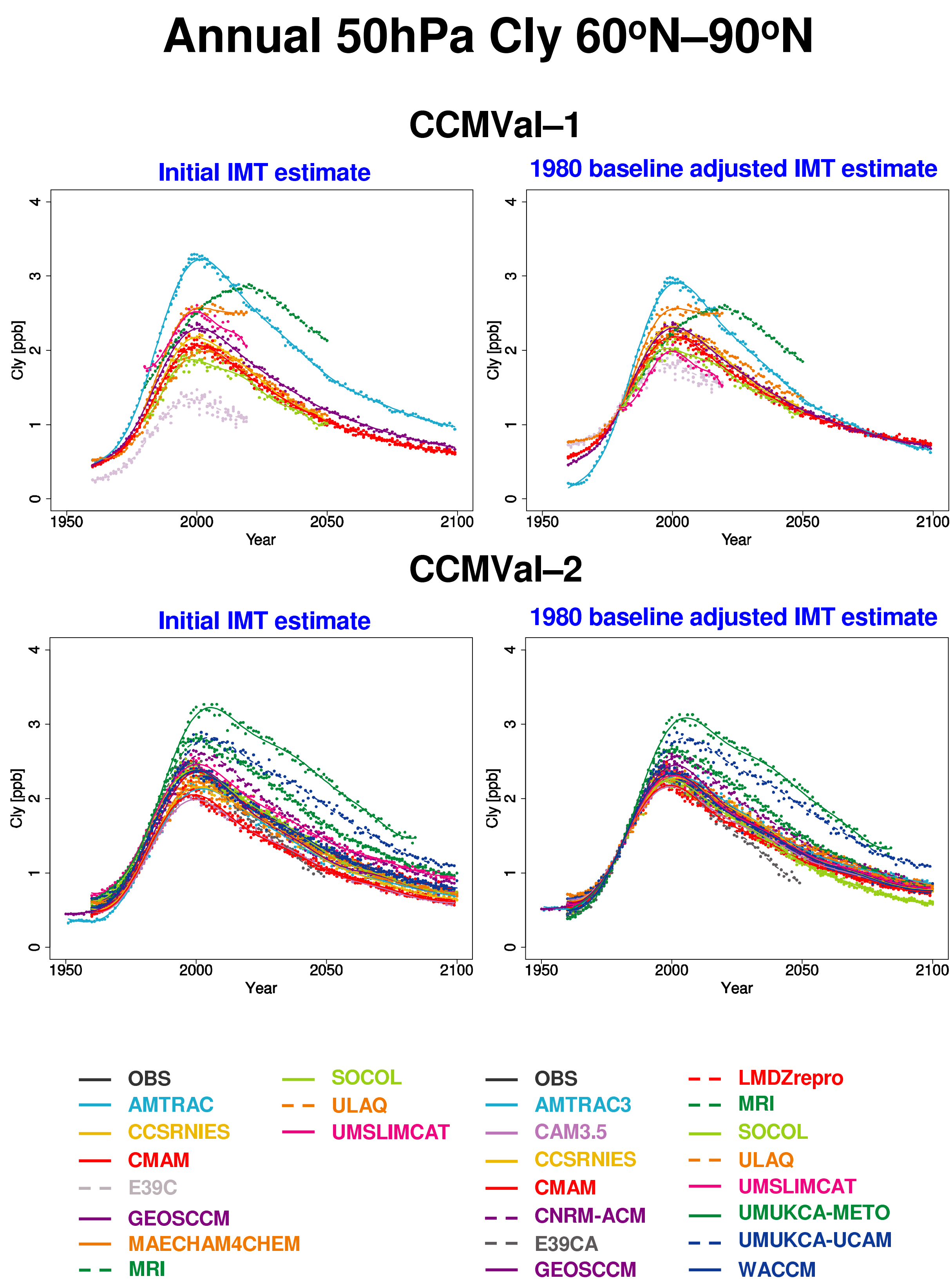

Figure 9S.29: As in Fig. 9S.5 but for the latitude range 60°N-90°N.

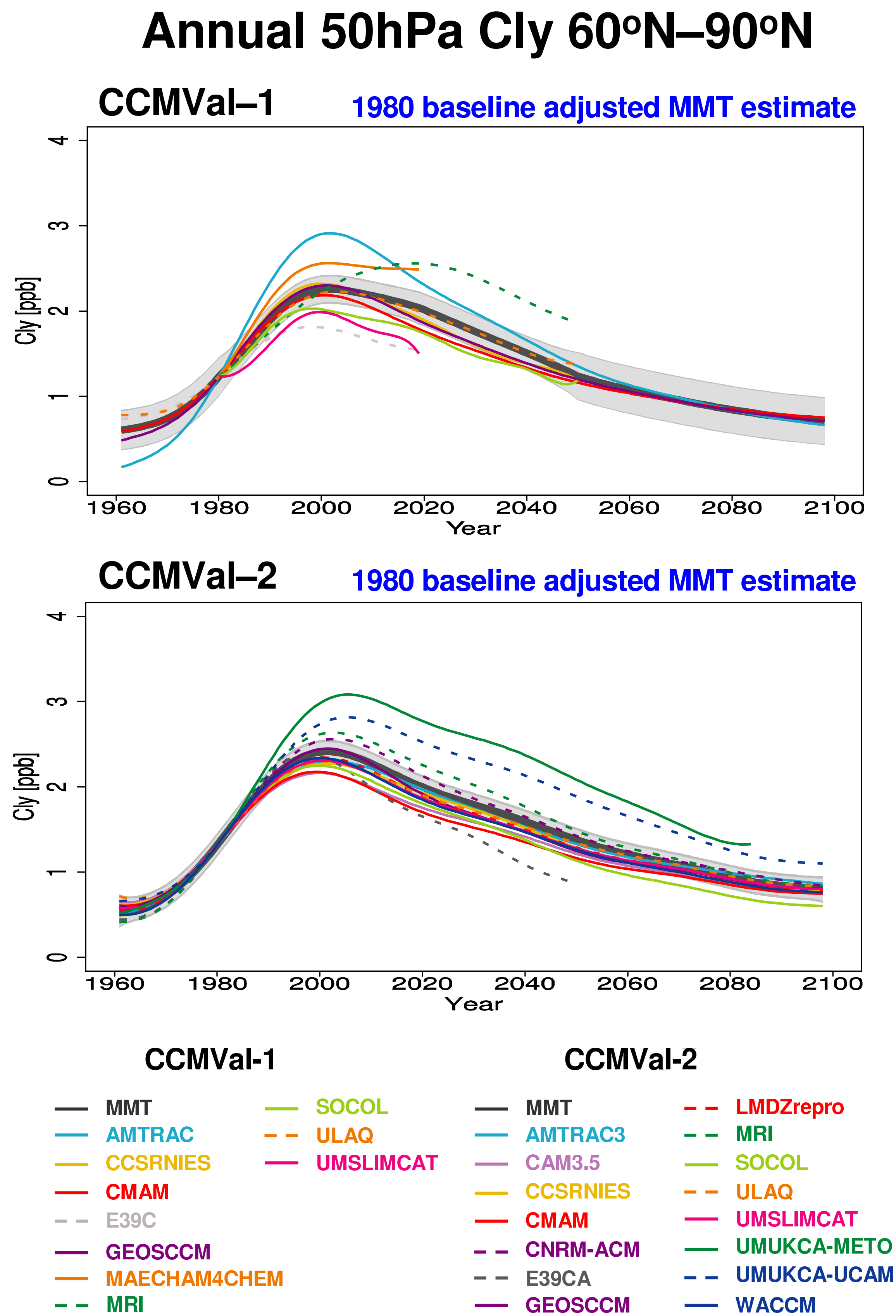

Figure 9S.30: As in Fig. 9S.6 but for the latitude range 60°N-90°N.

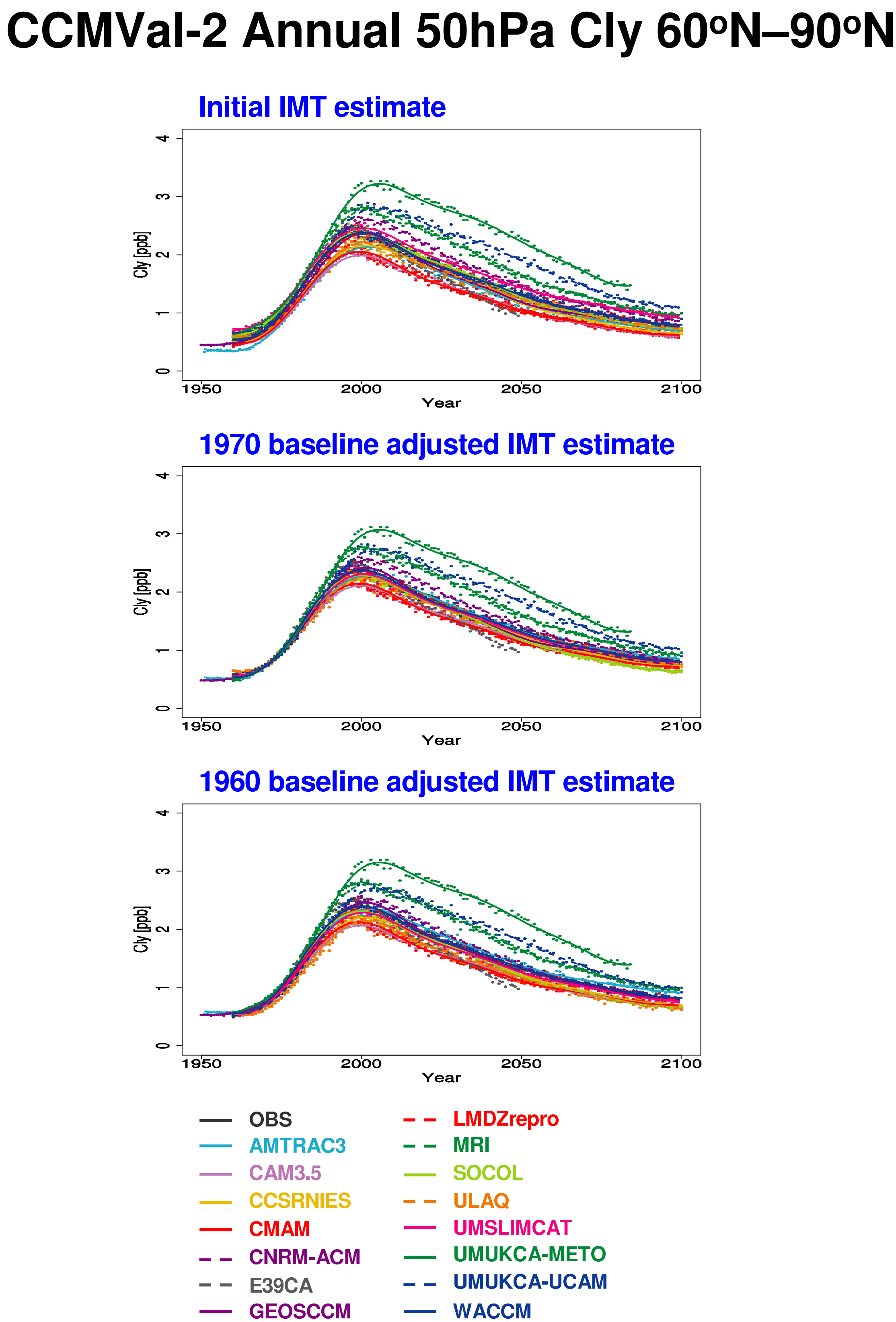

Figure 9S.31: As in Fig. 9S.7 but for the latitude range 60°N-90°N.

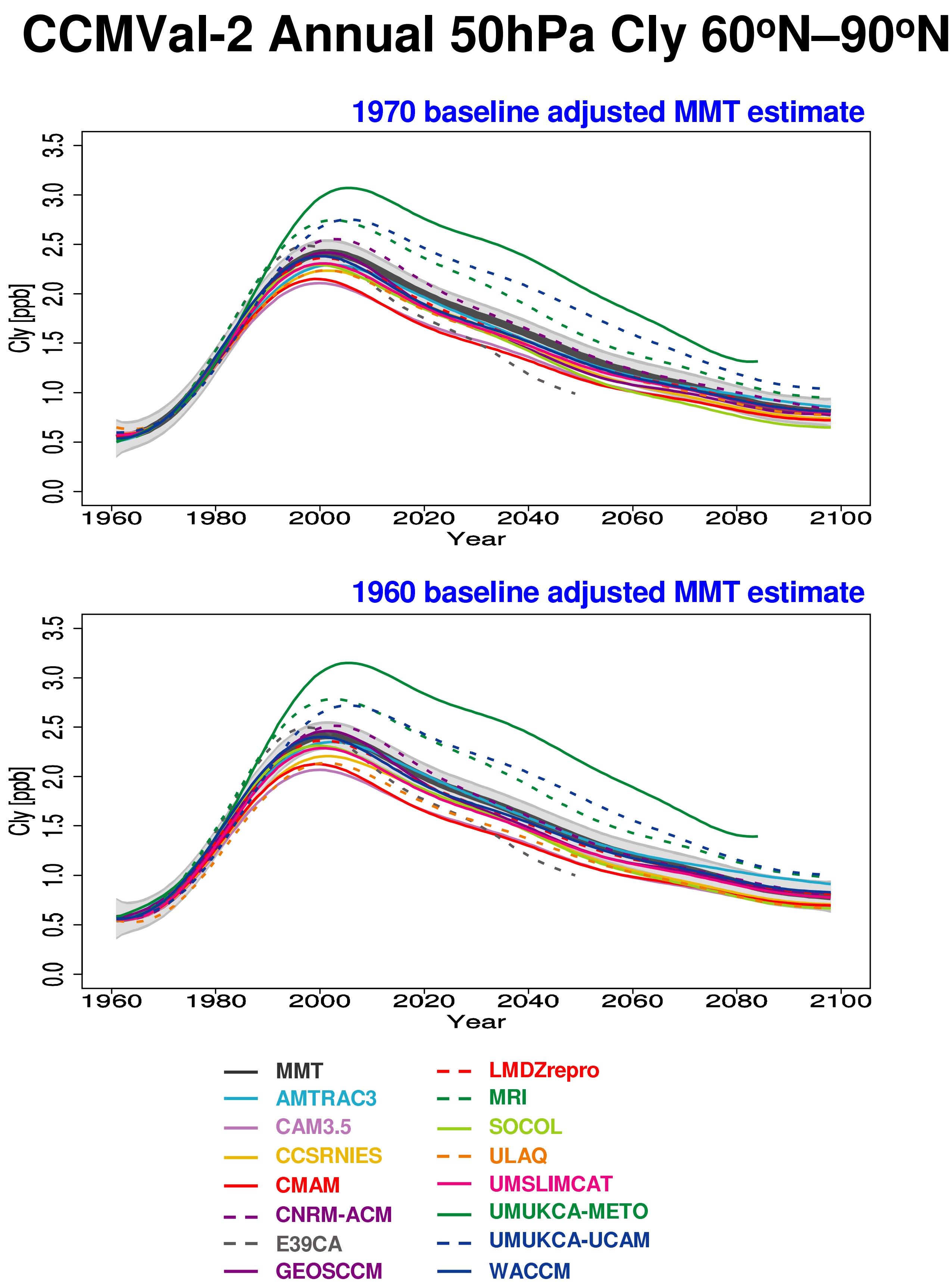

Figure 9S.32: As in Fig. 9S.8 but for the latitude range 60°N-90°N.

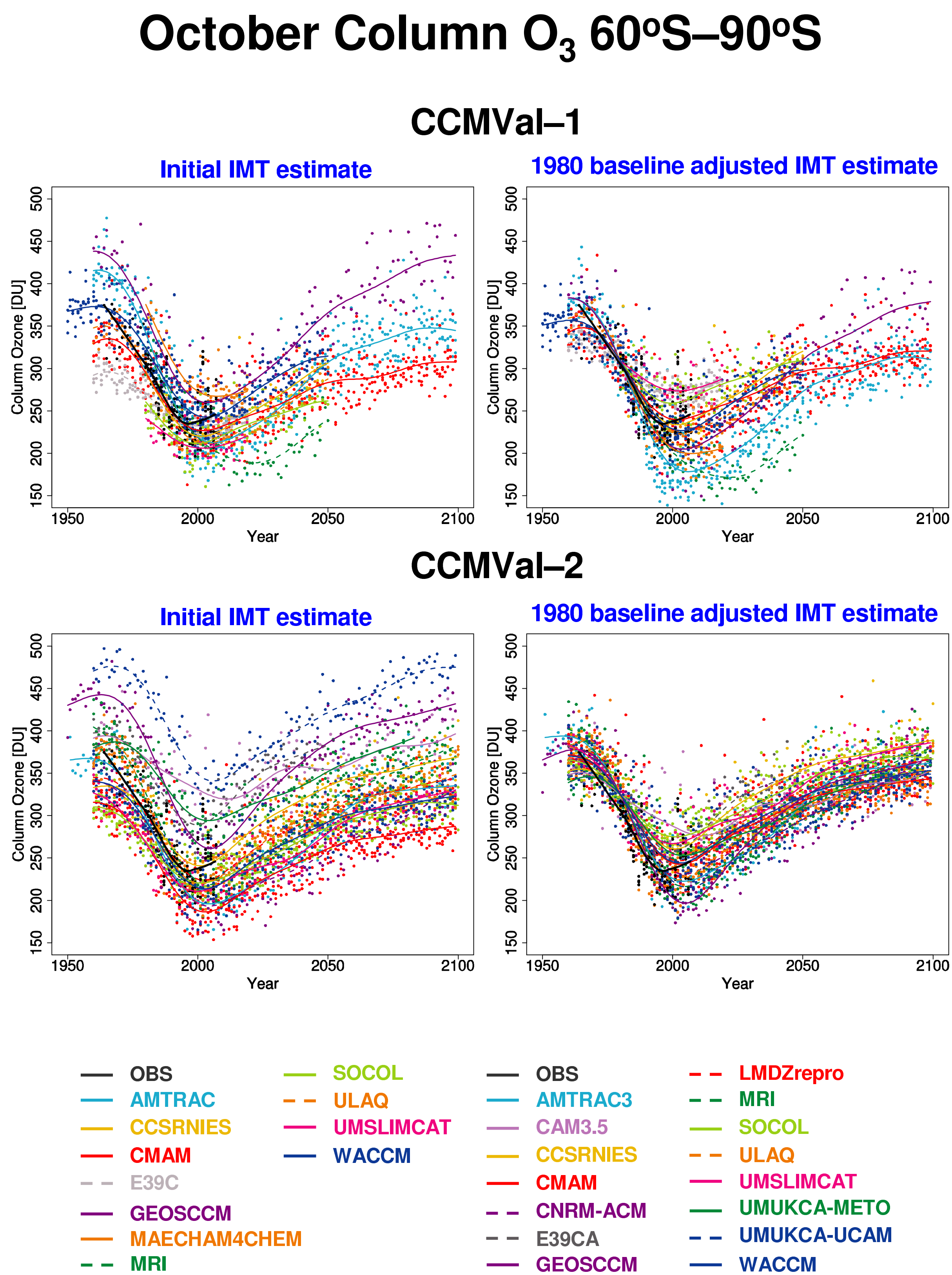

Figure 9S.33: As in Fig. 9S.1 but for the month of October and the latitude range 60°S-90°S.

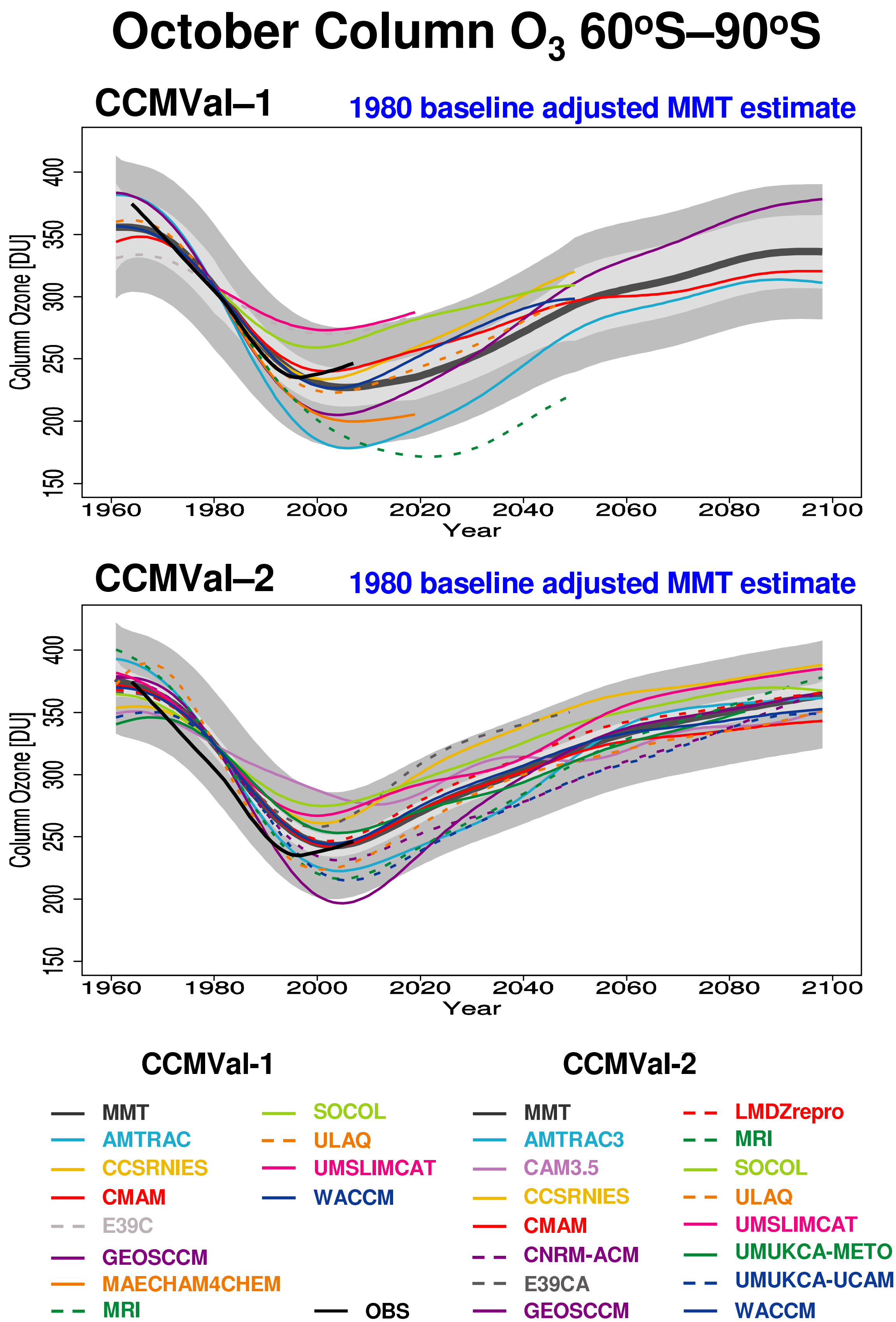

Figure 9S.34: As in Fig. 9S.2 but for the month of October and the latitude range 60°S-90°S.

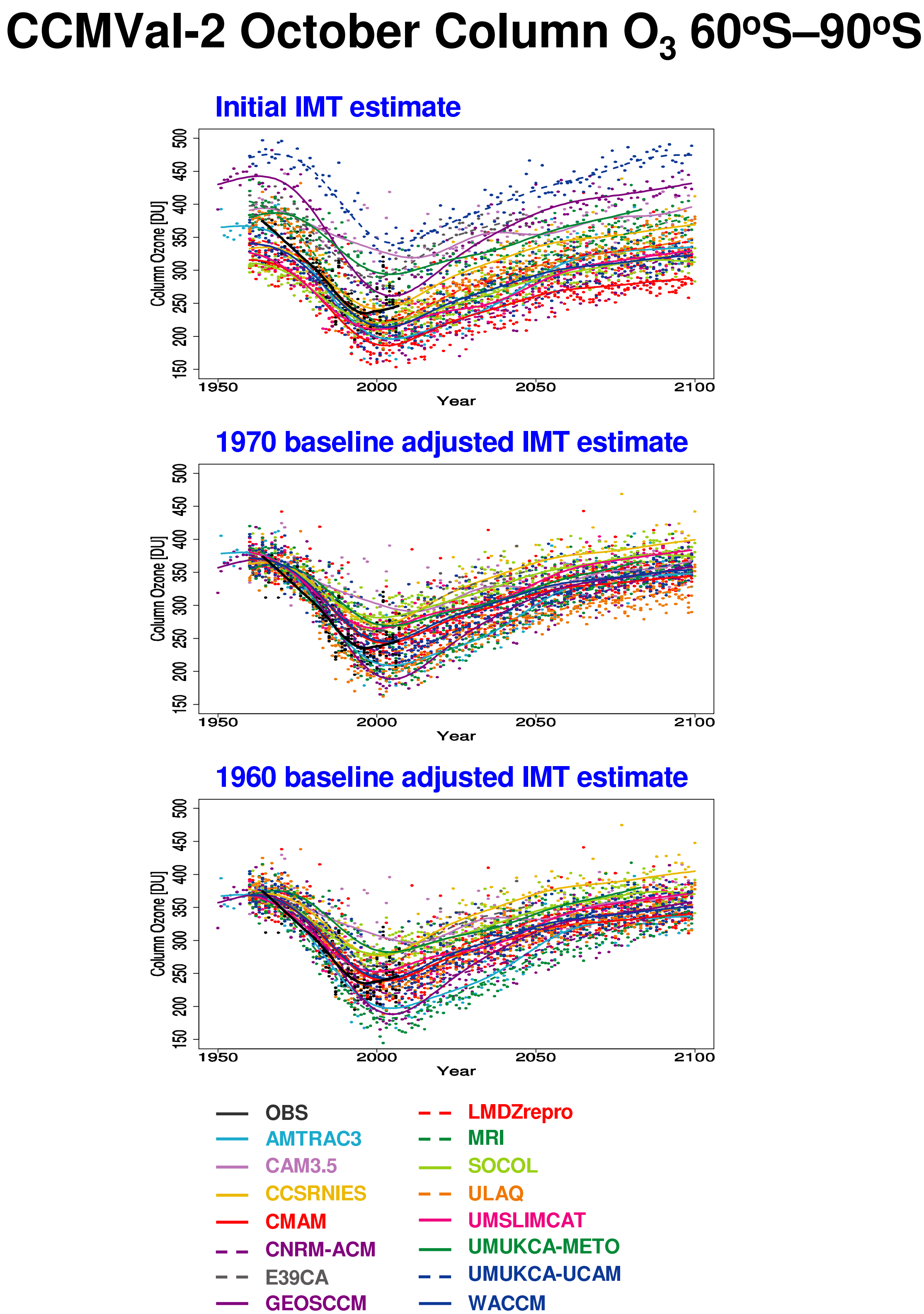

Figure 9S.35: As in Fig. 9S.3 but for the month of October and the latitude range 60°S-90°S.

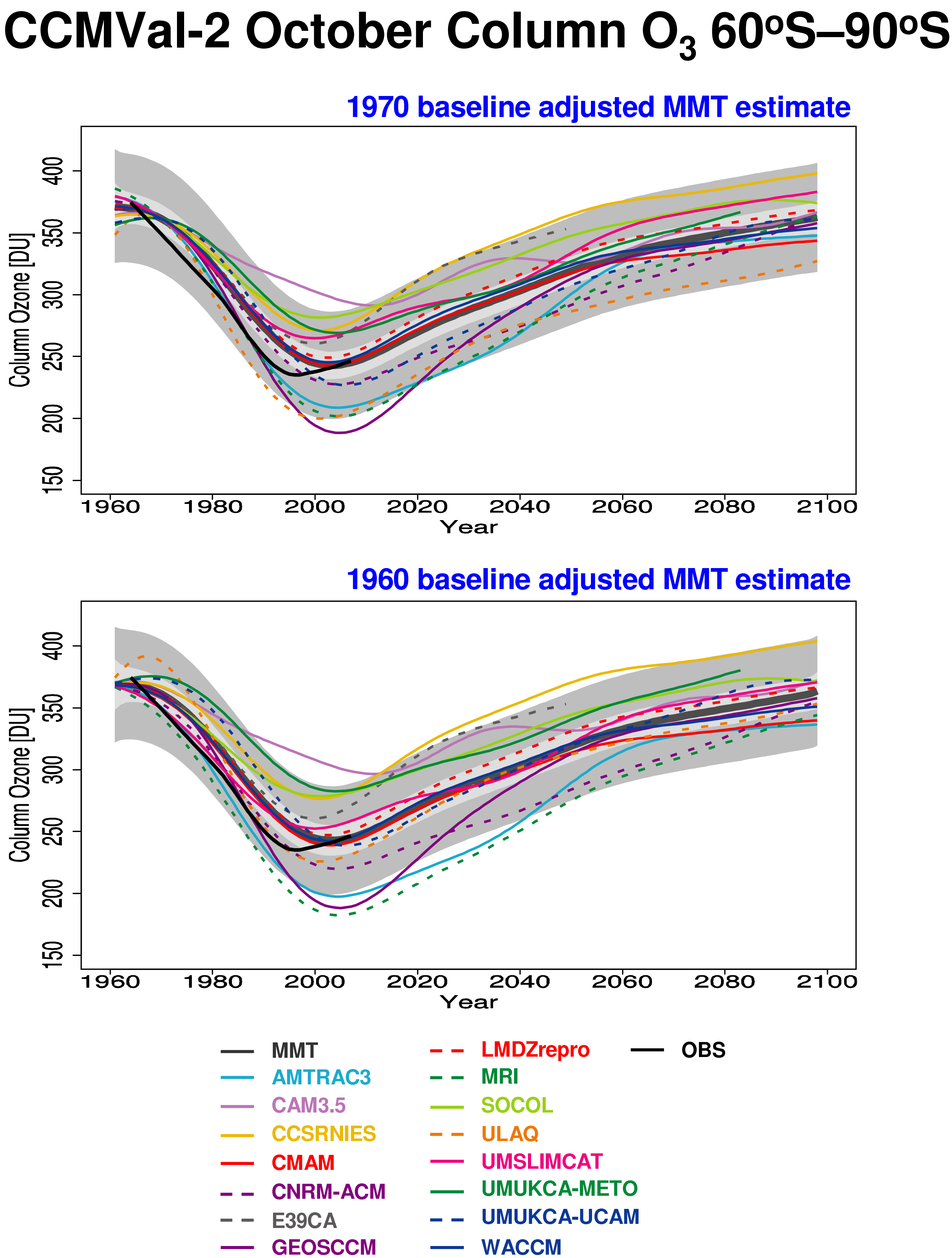

Figure 9S.36: As in Fig. 9S.4 but for the month of October and the latitude range 60°S-90°S.

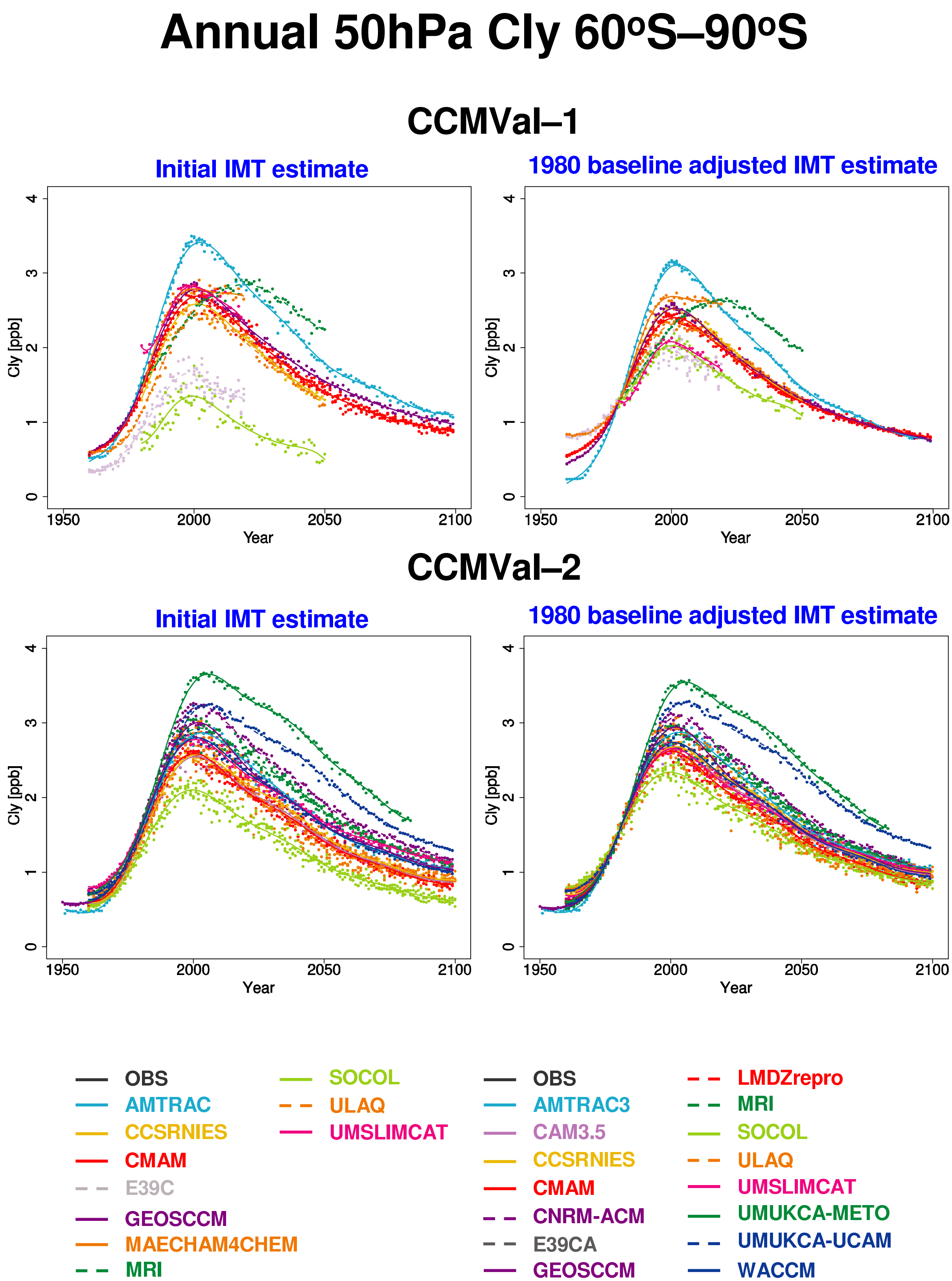

Figure 9S.37: As in Fig. 9S.5 but for the latitude range 60°S-90°S.

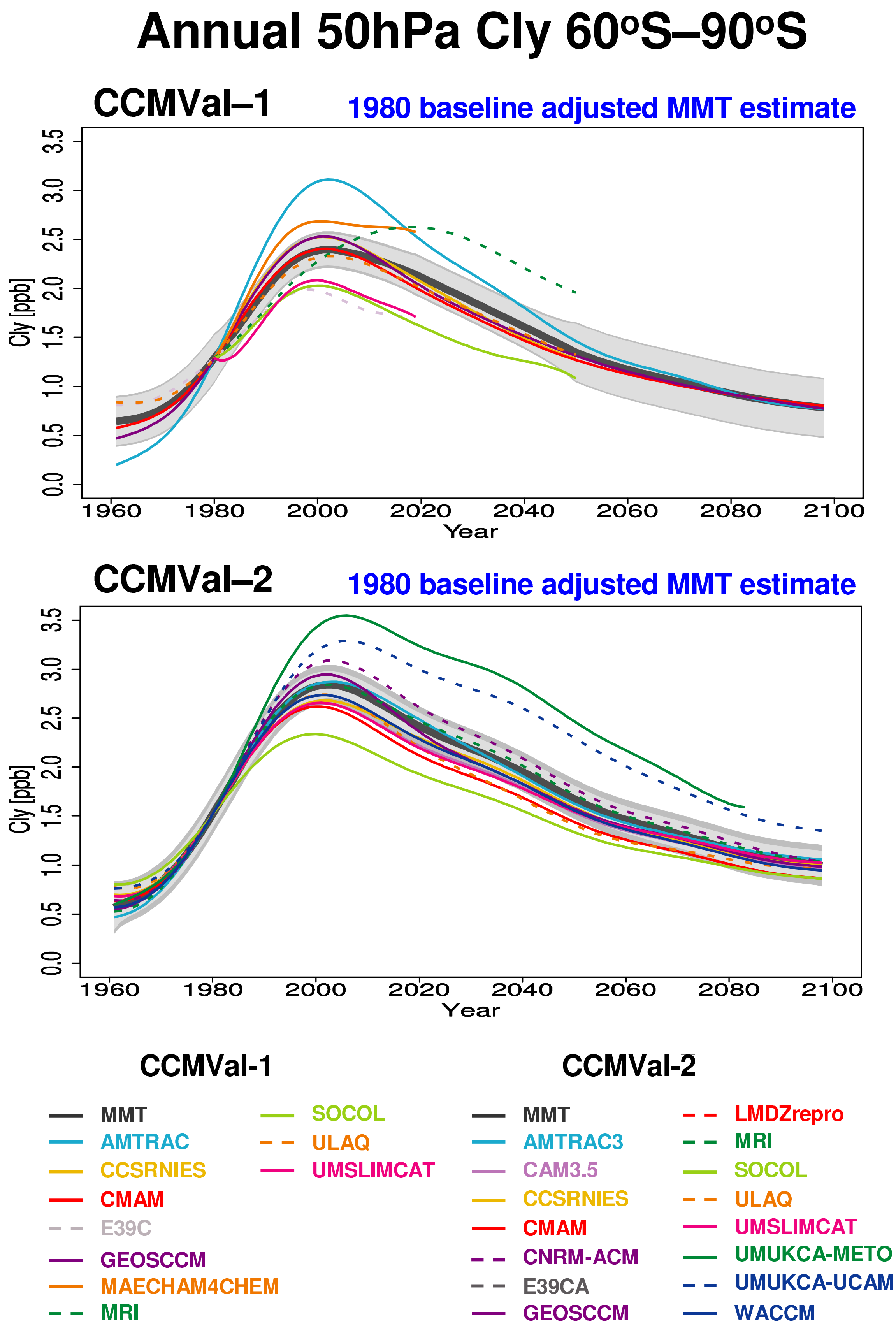

Figure 9S.38: As in Fig. 9S.6 but for the latitude range 60°S-90°S.

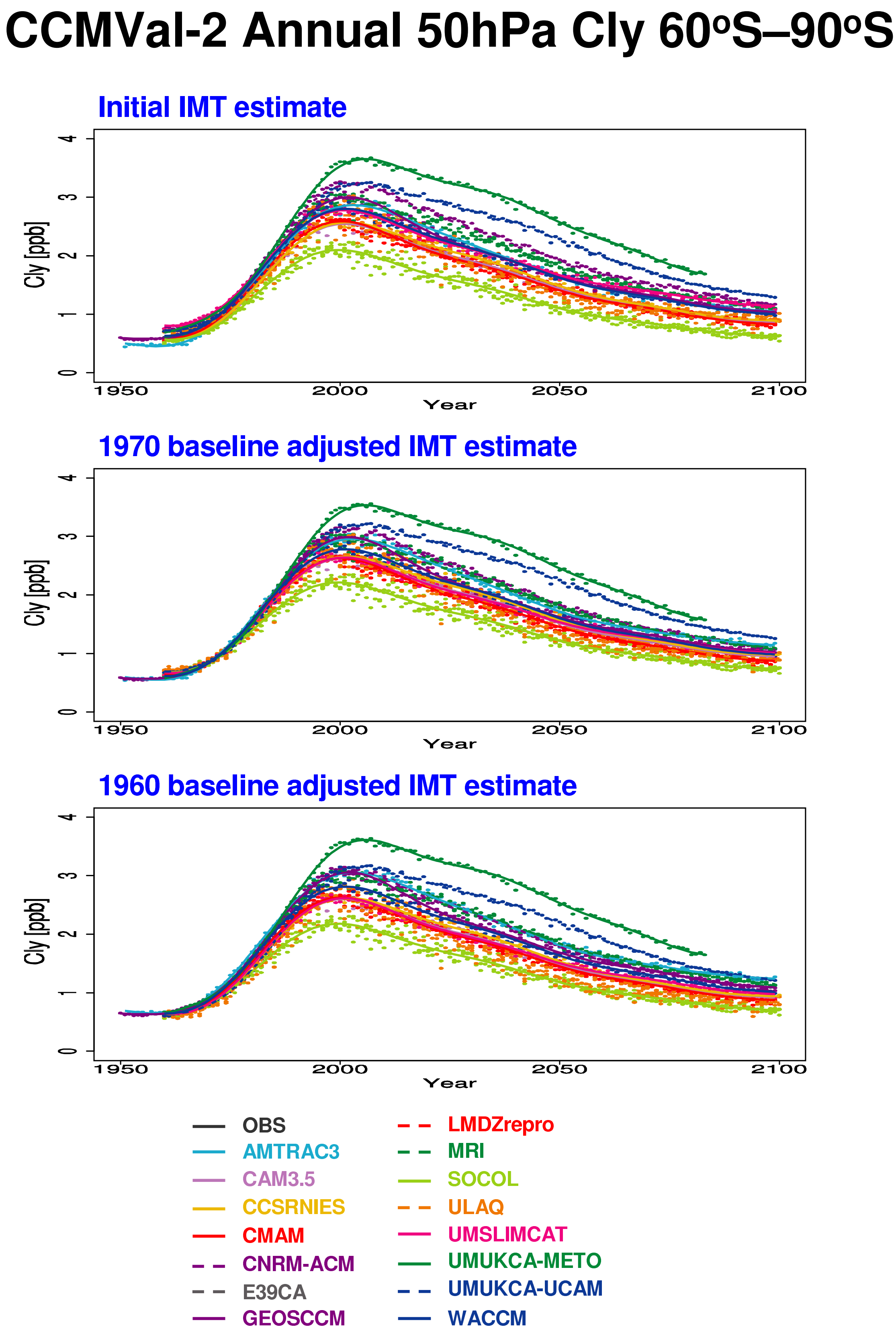

Figure 9S.39: As in Fig. 9S.7 but for the latitude range 60°S-90°S.

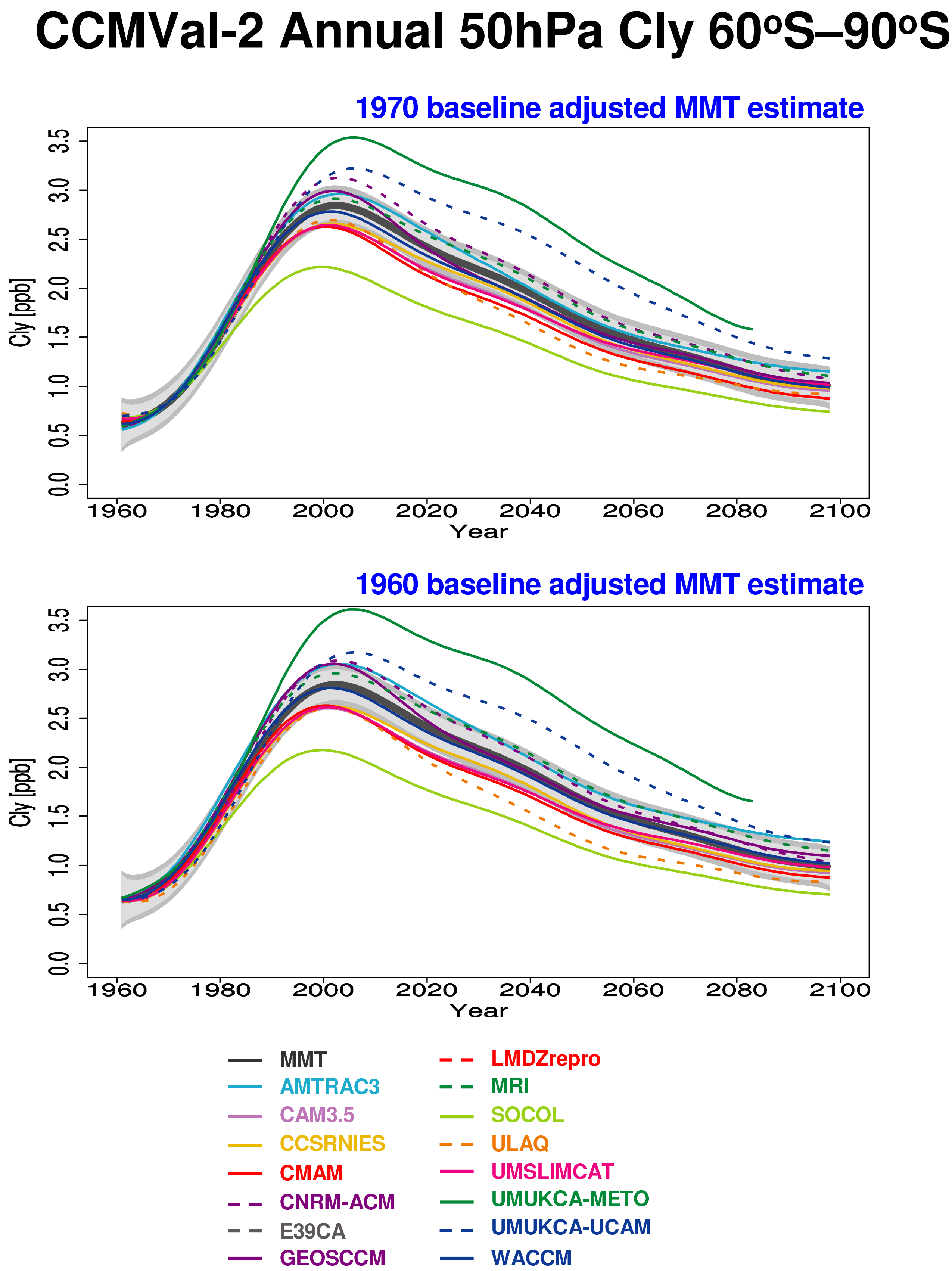

Figure 9S.40: As in Fig. 9S.8 but for the latitude range 60°S-90°S.

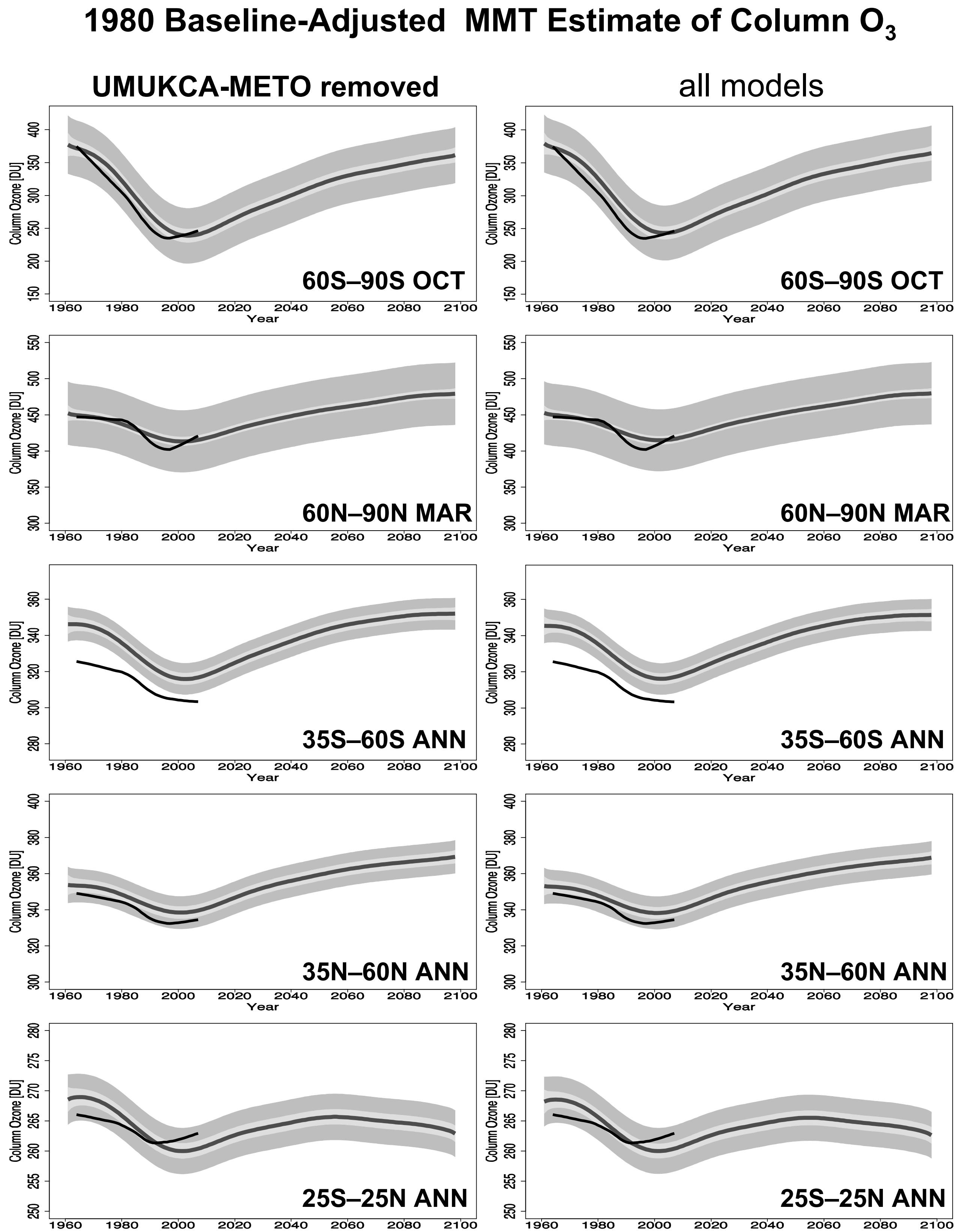

Figure 9S.41: MMT estimates and their 95% confidence and 95% prediction intervals for total Column O_3 in the 5 latitude bands considered in Chapter 9. The right-hand column shows the TSAM analysis applied to all models while the left hand column shows the same analysis but with the UMUKCA-METO model removed.

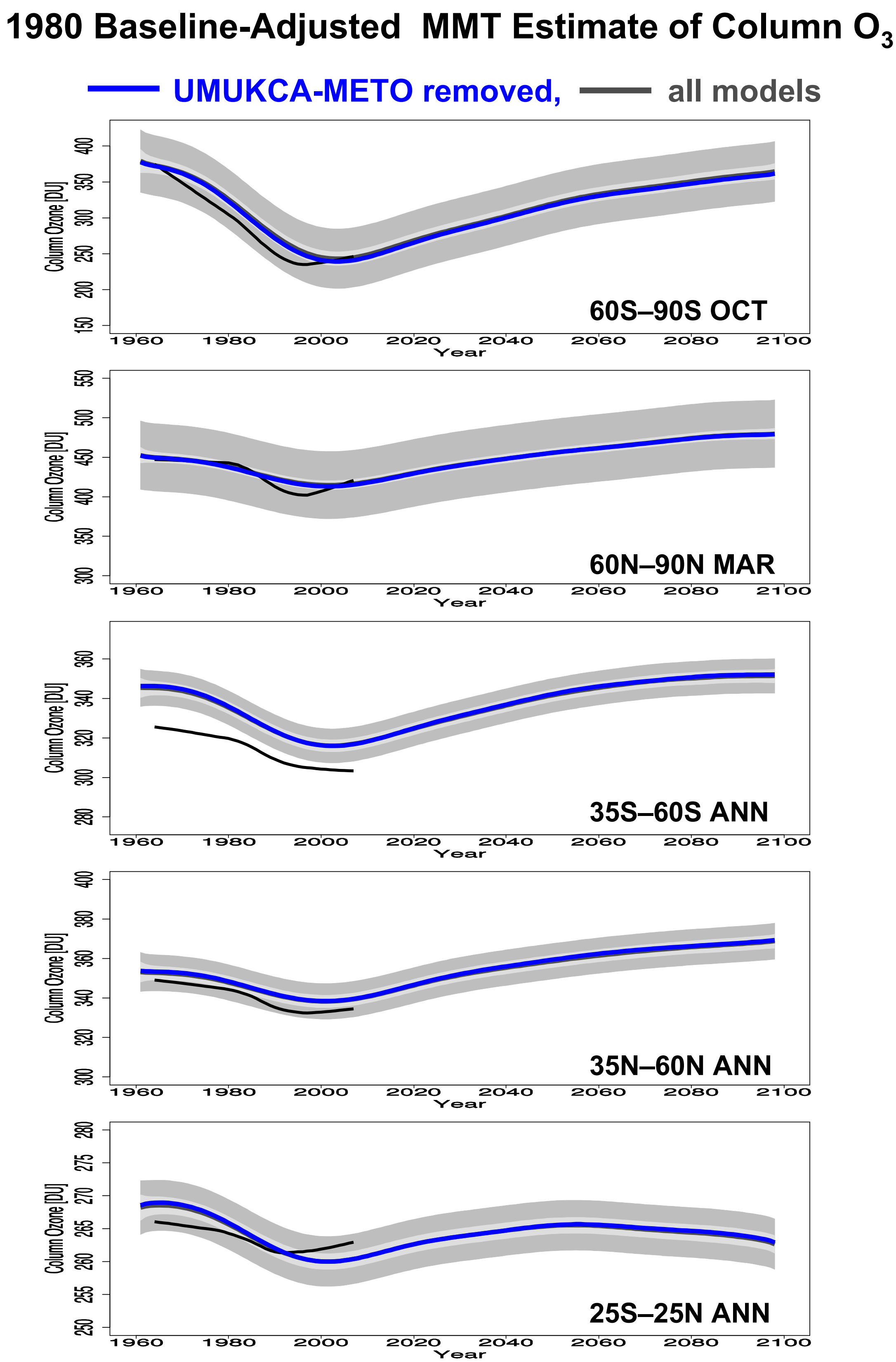

Figure 9S.42: MMT estimates of total column O_3 from the TSAM analysis applied to all models (dark grey lines) and their 95% confidence and 95% prediction intervals overlaid by the MMT estimate from the same TSAM analysis applied to all models except UMUKCA-METO (blue lines).

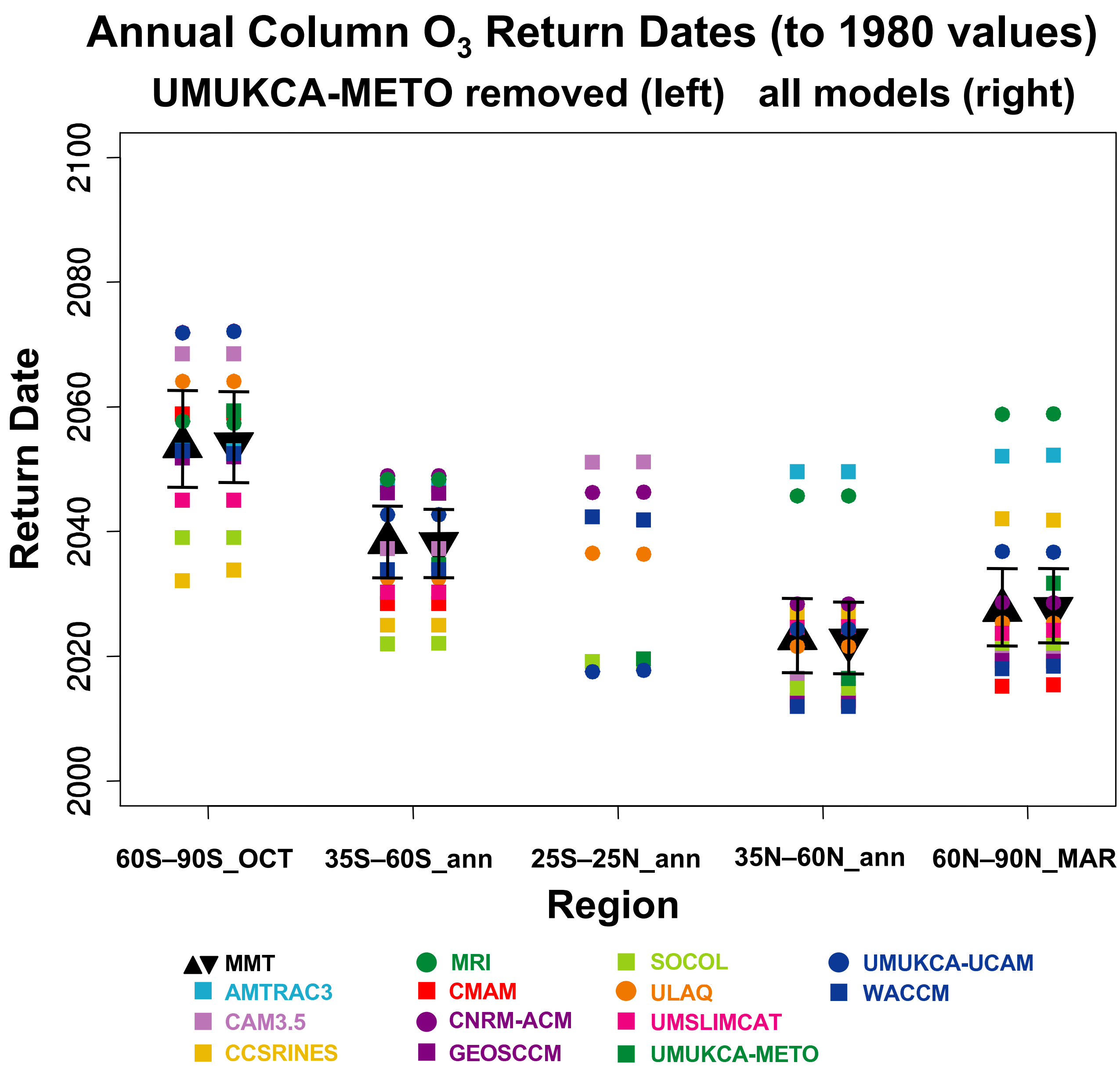

Figure 9S.43: Date of return to 1980 values for the annual average (tropical and midlatitude) and spring (polar) total ozone column derived from the IMT (coloured symbols) and MMT (large black triangles) estimates for all CCMVal-2 models (right) and all models except UMUKCA-METO (left). The error bars on the MMT estimates of recovery date are derived from the 95% confidence interval of the MMT estimates to the 1980 baseline-adjusted time series data.

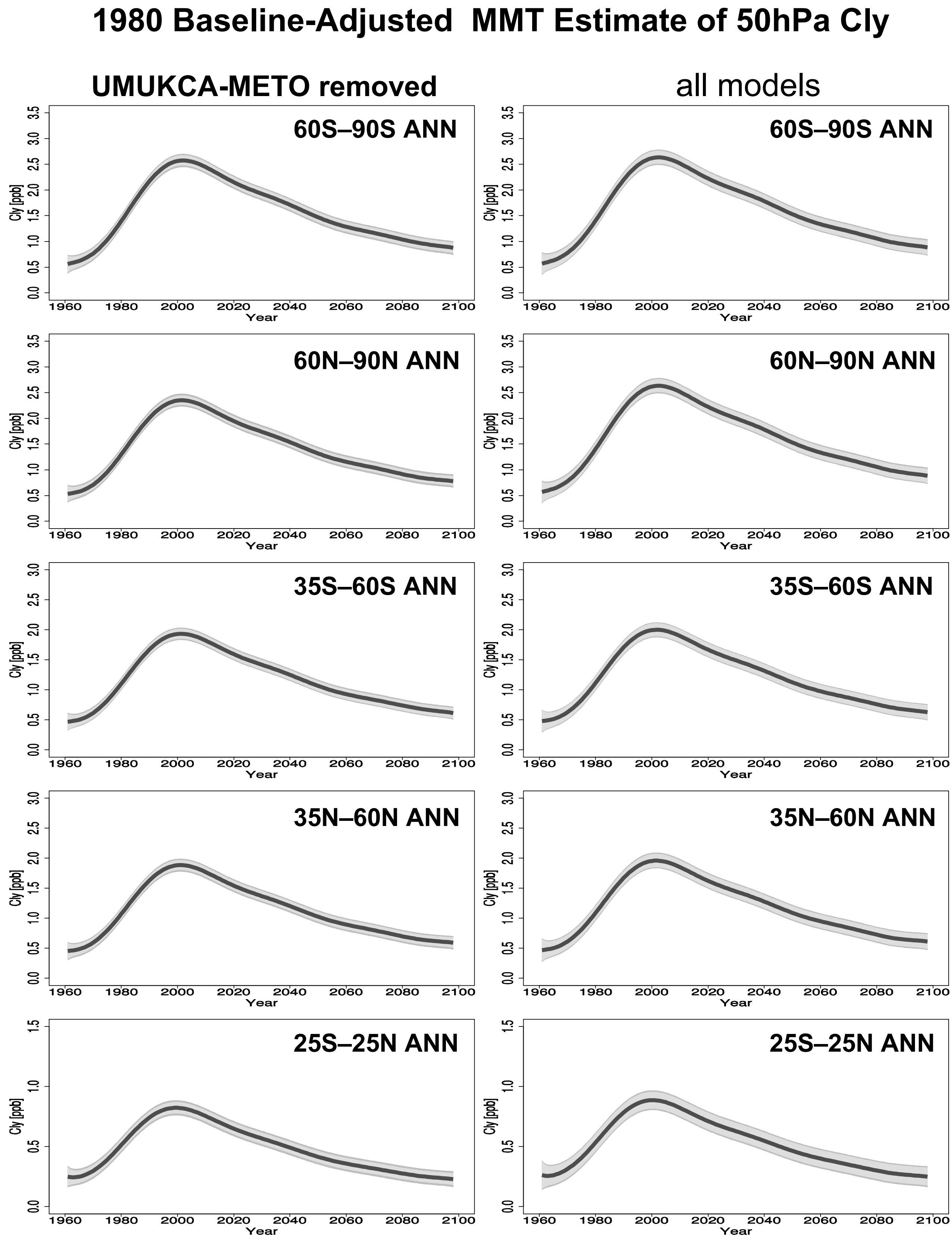

Figure 9S.44: MMT estimates and their 95% confidence and 95% prediction intervals for 50hPa Cly in the 5 latitude bands considered in Chapter 9. The right-hand column shows the TSAM analysis applied to all models while the left hand column shows the same analysis but with the UMUKCA-METO model removed.

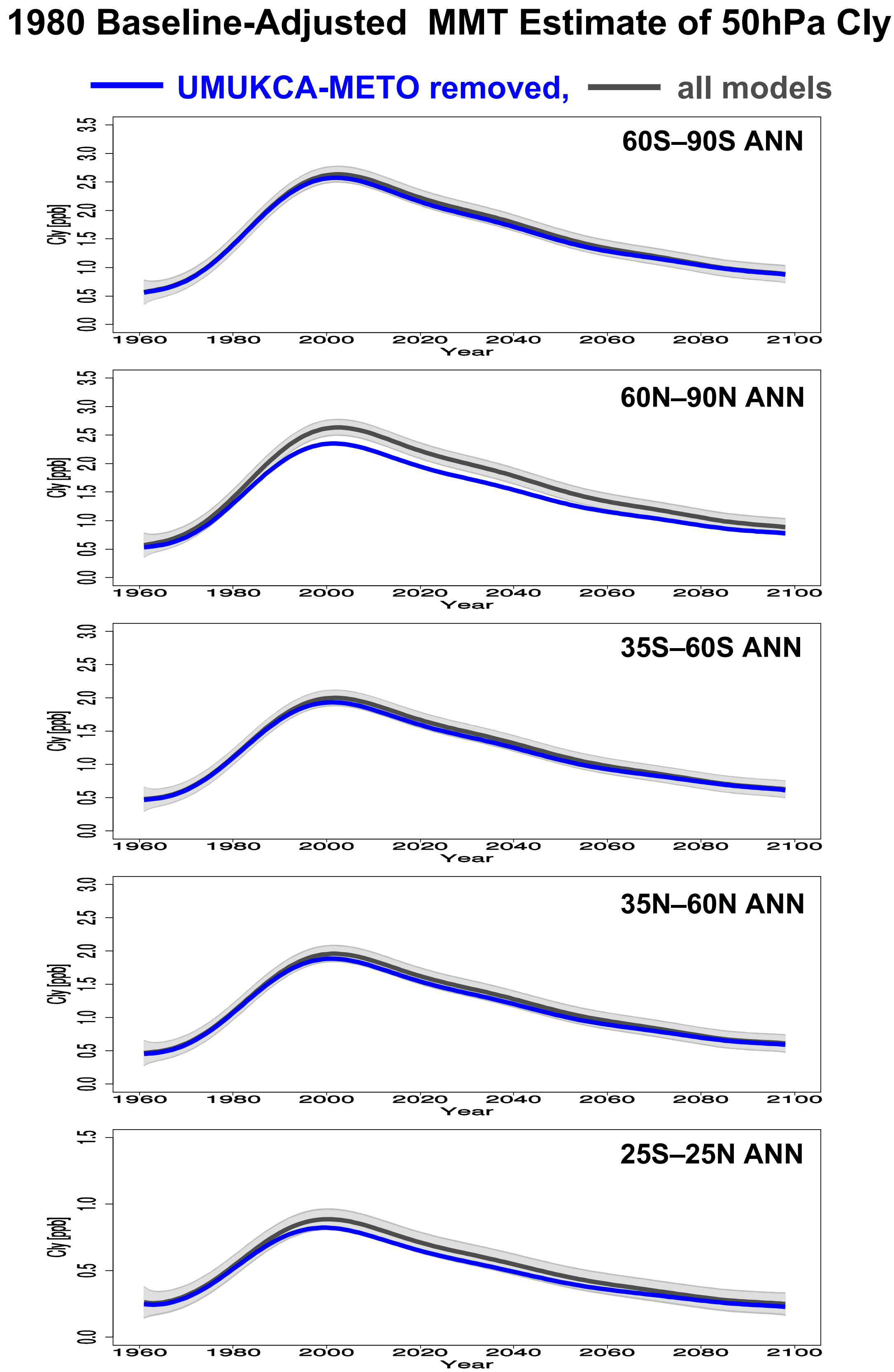

Figure 9S.45: MMT estimates of 50hPa Cly from the TSAM analysis applied to all models (dark grey lines) and their 95% confidence and 95% prediction intervals overlaid by the MMT estimate from the same TSAM analysis applied to all models except UMUKCA-METO (blue lines).

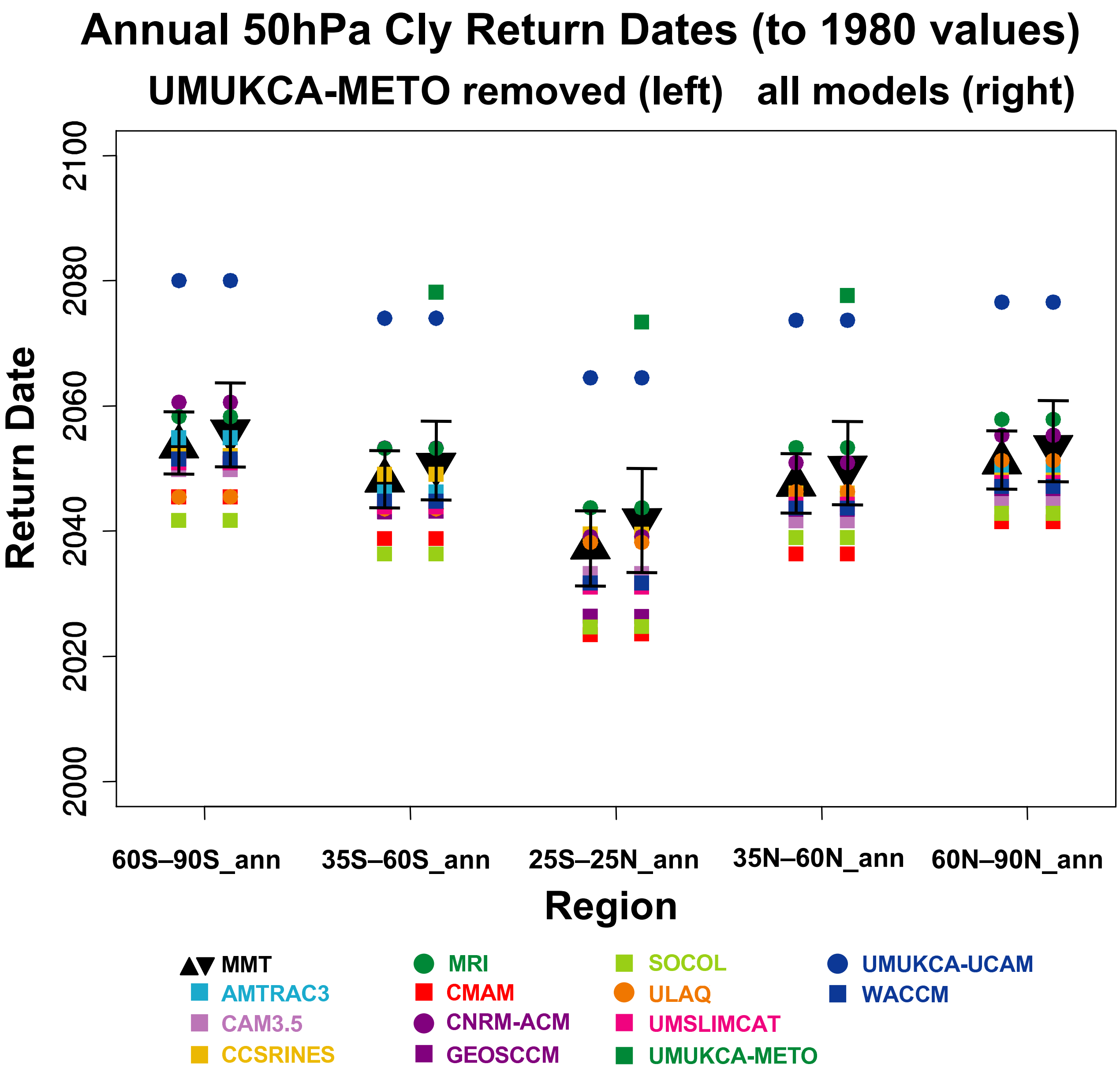

Figure 9S.46: Date of return to 1980 values for the annual average 50hPa Cly derived from the IMT (coloured symbols) and MMT (large black triangles) estimates for all CCMVal-2 models (right) and all models except UMUKCA-METO (left). The error bars on the MMT estimates of recovery date are derived from the 95% confidence interval of the MMT estimates to the 1980 baseline-adjusted time series data.

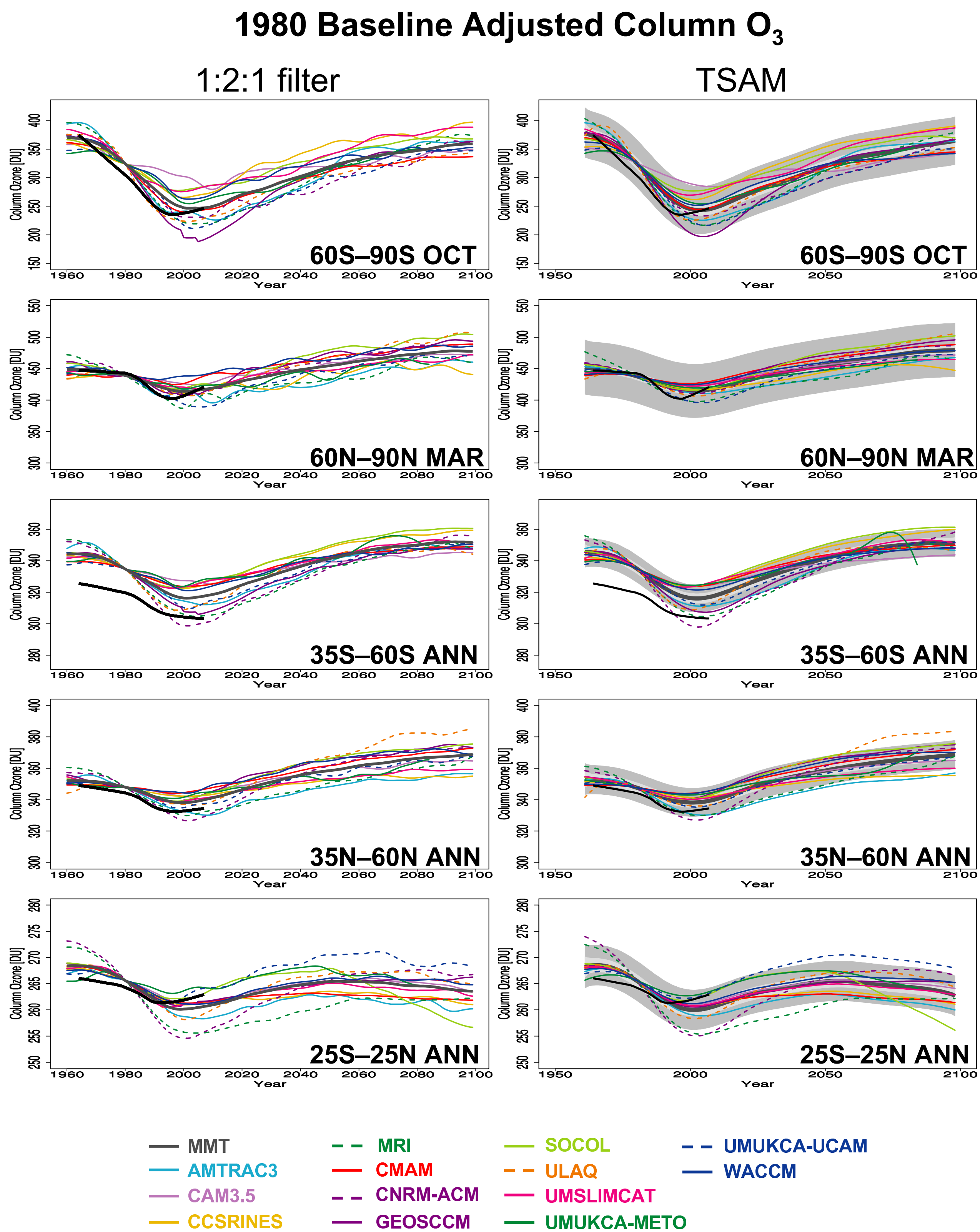

Figure 9S.47: Comparison of IMT estimates derived from a 1:2:1 filter applied 30 times (left) and the TSAM analysis (right) for total Column O_3 in the 5 latitude bands considered in Chapter 9. The multi-model trend derived from an average over the smooth IMT estimates (left) and TSAM procedure (right) are plotted as dark grey lines. 95% confidence and 95% prediction intervals have been included for the TSAM analysis (right).

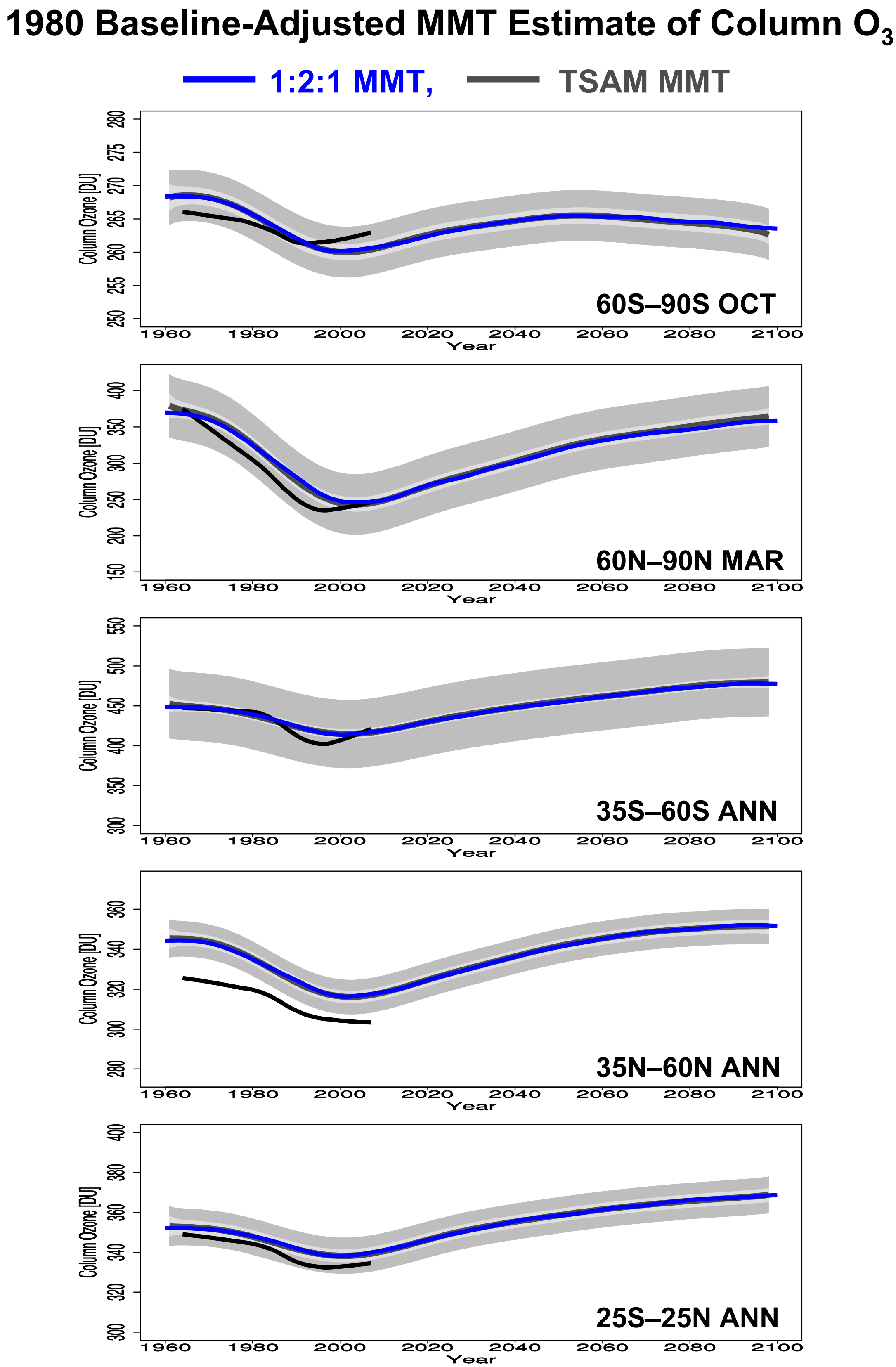

Figure 9S.48: MMT estimates of total column O_3 from the TSAM analysis (dark grey lines) and their 95% confidence and 95% prediction intervals overlaid by the MMT estimate derived from 1:2:1 smoothing presented Fig. 9S.47 (blue lines).

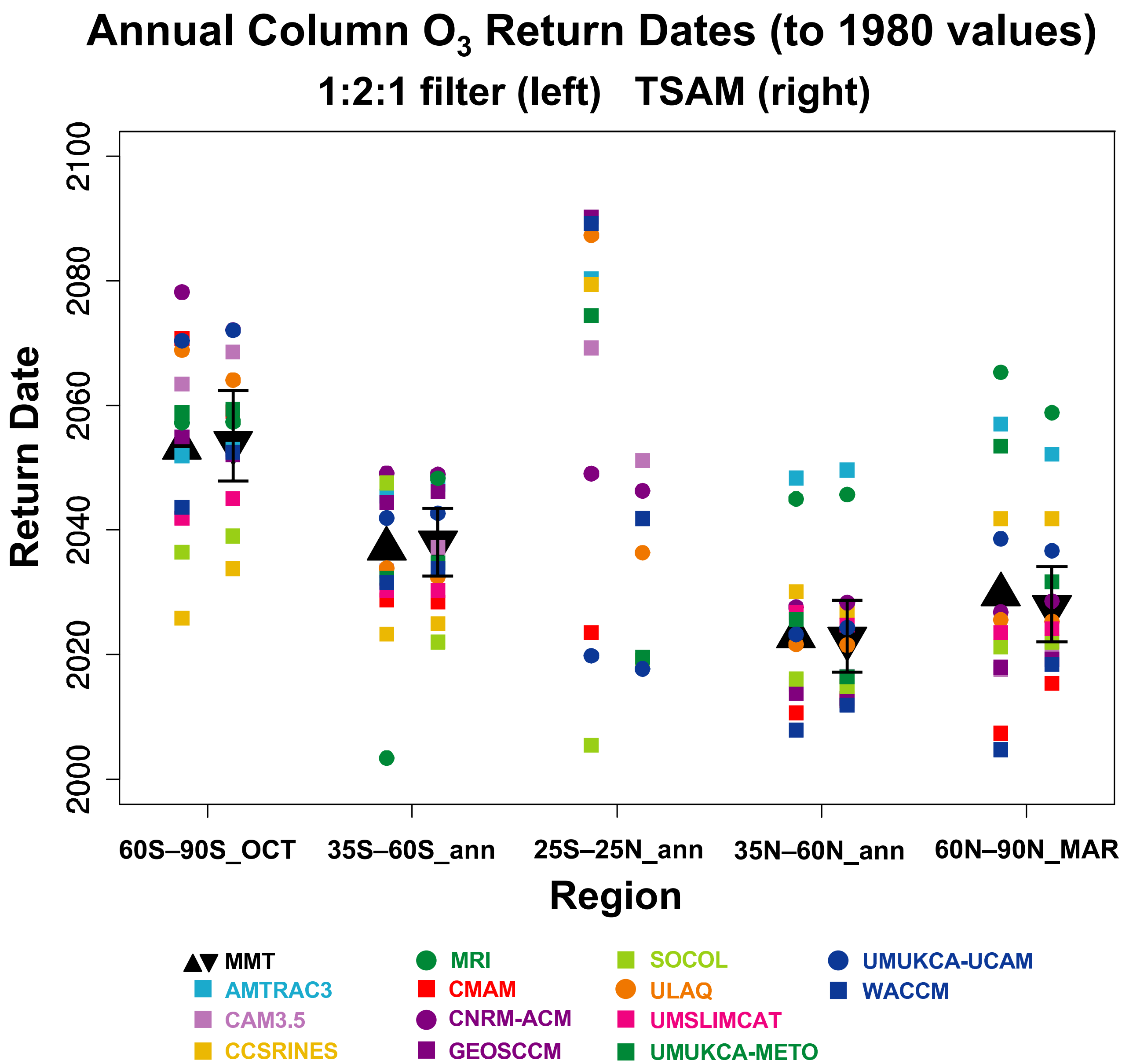

Figure 9S.49: Date of return to 1980 values for the annual average (tropical and midlatitude) and spring (polar) total ozone column derived from the IMT (coloured symbols) and MMT (large black triangles) estimates using 1:2:1 smoothing (left) and the TSAM analysis (right). The error bars on the MMT estimates of recovery date are derived from the TSAM 95% confidence interval of the MMT estimates to the 1980 baseline-adjusted time series data.

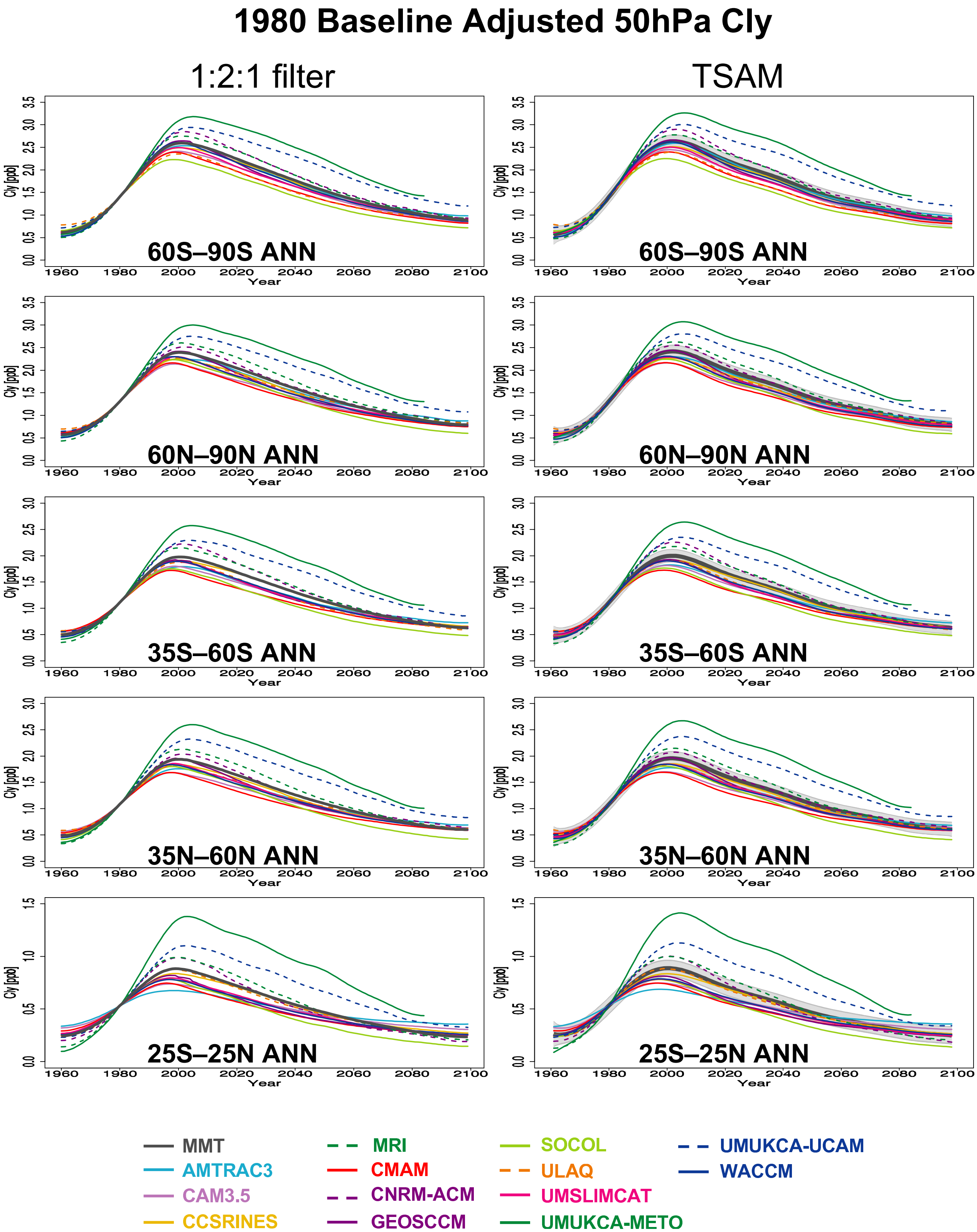

Figure 9S.50: Comparison of IMT estimates derived from a 1:2:1 filter applied 30 times (left) and the TSAM analysis (right) for 50hPa Cly in the 5 latitude bands considered in Chapter 9. The multi-model trend derived from an average over the smooth IMT estimates (left) and TSAM procedure (right) are plotted as dark grey lines. 95% confidence and 95% prediction intervals have been included for the TSAM analysis (right).

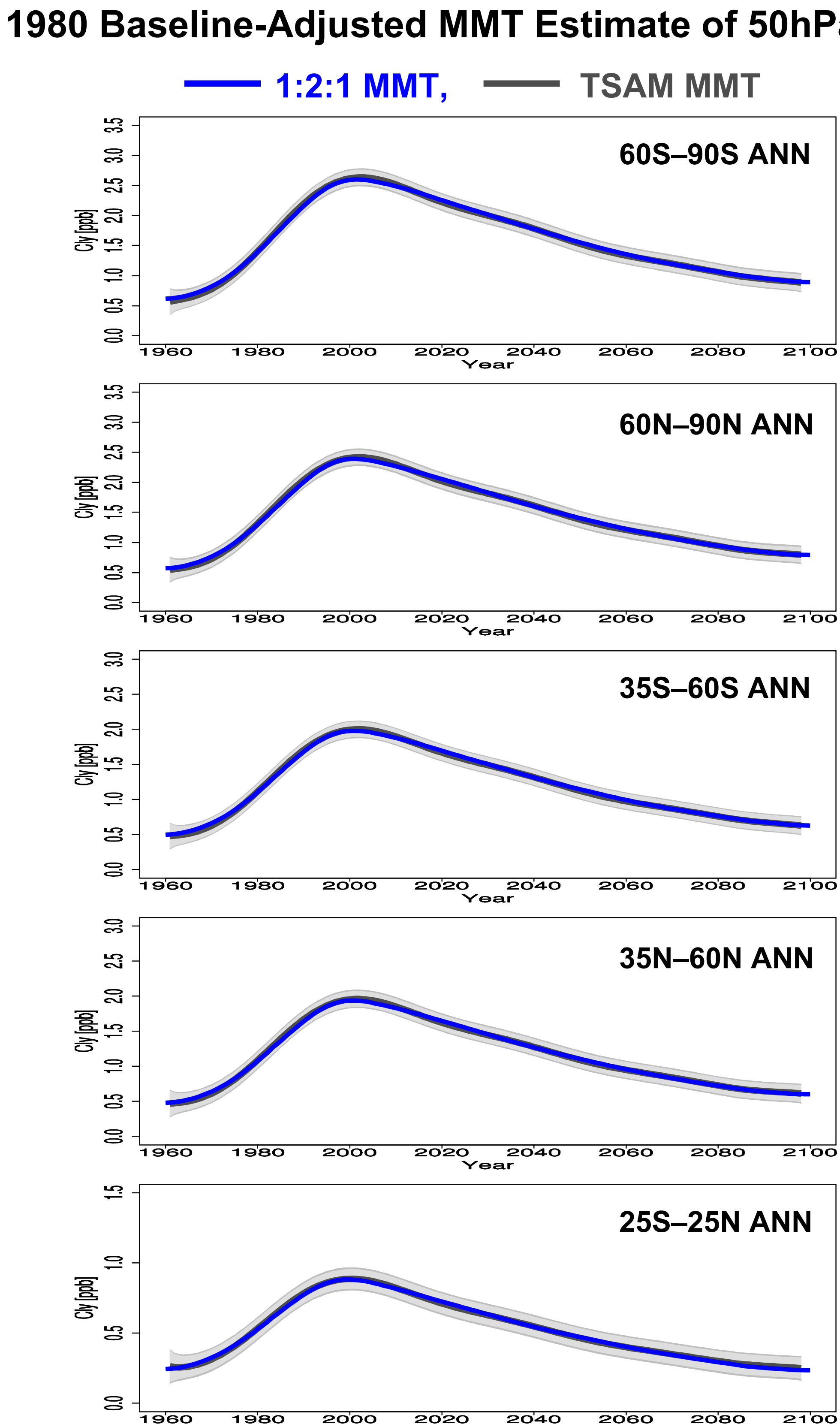

Figure 9S.51: MMT estimates of 50hPa Cly from the TSAM analysis (dark grey lines) and their 95% confidence and 95% prediction intervals overlaid by the MMT estimate derived from 1:2:1 smoothing presented Fig. 9S.50 (blue lines).

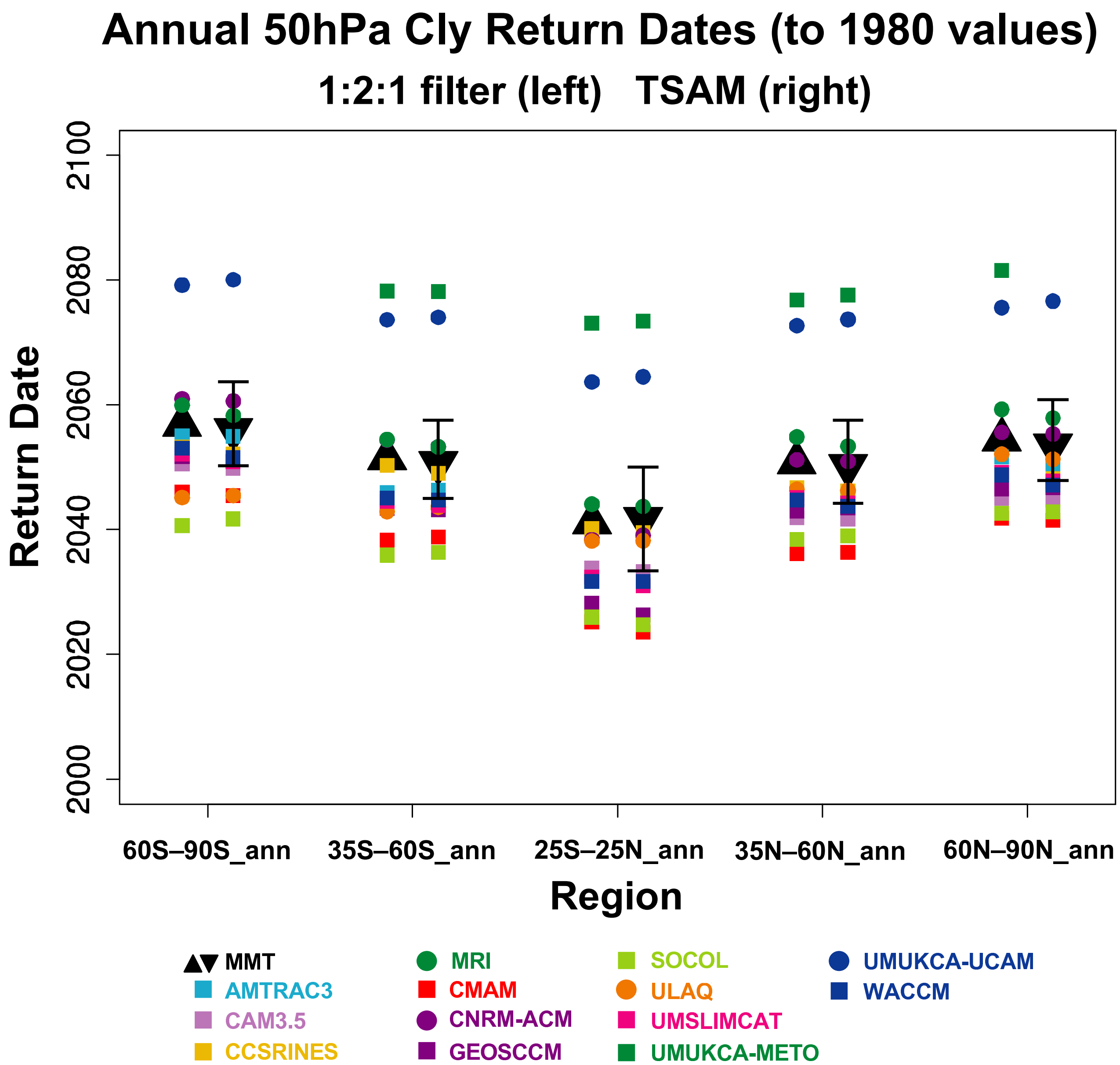

Figure 9S.52: Date of return to 1980 values for the annual average 50hPa Cly derived from the IMT (coloured symbols) and MMT (large black triangles) estimates using 1:2:1 smoothing (left) and the TSAM analysis (right). The error bars on the MMT estimates of recovery date are derived from the TSAM 95% confidence interval of the MMT estimates to the 1980 baseline-adjusted time series data.